Importance and vulnerability of the world's water towers

W. W. Immerzeel[1,2,26*], A. F. Lutz[1,2,26*], M. Andrade[3,4], A. Bahl[5], H. Biemans[6], T. Bolch[7], S. Hyde[5], S. Brumby[5], B. J. Davies[8], A. C. Elmore[5], A. Emmer[9], M. Feng[10], A. Fernández[11], U. Haritashya[12], J. S. Kargel[13], M. Koppes[14], P. D. A. Kraaijenbrink[1], A. V. Kulkarni[15], P. Mayewski[16], S. Nepal[17], P. Pacheco[18], T. H. Painter[19], F. Pellicciotti[20], H. Rajaram[21], S. Rupper[22], A. Sinisalo[17], A. B. Shrestha[17], D. Viviroli[23], Y. Wada[24], C. Xiao[25], T. Yao[10] & J. E. M. Baillie[5]

[1]Faculty of Geosciences, Department of Physical Geography, Utrecht University, Utrecht, The Netherlands.

[2]FutureWater, Wageningen, The Netherlands.

[3]Universidad Mayor de San Andrés, Institute for Physics Research, La Paz, Bolivia.

[4]University of Maryland, Department of Atmospheric and Oceanic Science, College Park, MD, USA.

[5]National Geographic Society, Washington, DC, USA.

[6]Wageningen University and Research, Water and Food Research Group, Wageningen, The Netherlands.

[7]School of Geography and Sustainable Development, University of St Andrews, St Andrews, UK.

[8]Centre for Quaternary Research, Department of Geography, Royal Holloway University of London, Egham, UK.

[9]Czech Academy of Sciences, Global Change Research Institute, Brno, Czech Republic.

[10]Institute of Tibetan Plateau Research, Chinese Academy of Sciences, Beijing, China.

[11]Department of Geography, Universidad de Concepción, Concepción, Chile.

[12]Department of Geology, University of Dayton, Dayton, OH, USA.

[13]Department of Hydrology and Atmospheric Sciences, University of Arizona, Tucson, AZ, USA.

[14]Department of Geography, University of British Columbia, Vancouver, British Columbia, Canada.

[15]Indian Institute of Science, Divecha Center for Climate Change, Bangalore, India.

[16]University of Maine, Climate Change Institute, Orono, ME, USA.

[17]International Centre for Integrated Mountain Development, Kathmandu, Nepal.

[18]Agua Sustentable, Irpavi, La Paz, Bolivia.

[19]Joint Institute for Regional Earth System Science and Engineering, University of California, Los Angeles, CA, USA.

[20]Swiss Federal Research Institute WSL, Birmensdorf, Switzerland.

[21]Johns Hopkins University, Department of Environmental Health and Engineering, Baltimore, MD, USA.

[22]University of Utah, Department of Geography, Salt Lake City, UT, USA.

[23]University of Zurich, Department of Geography, Zurich, Switzerland.

[24]International Institute for Applied Systems Analysis, Laxenburg, Austria.

[25]State Key Laboratory of Earth Surface Processes and Resource Ecology, Beijing Normal University, Beijing, China.

[26]These authors contributed equally: W. W. Immerzeel, A. F. Lutz.

*e-mail: w.w.immerzeel@uu.nl; a.f.lutz@uu.nl.

ABSTRACT

Mountains are the water towers of the world, supplying a substantial part of both natural and anthropogenic water demands[1,2]. They are highly sensitive and prone to climate change[3,4], yet their importance and vulnerability have not been quantified at the global scale. Here we present a global water tower index (WTI), which ranks all water towers in terms of their water-supplying role and the downstream dependence of ecosystems and society. For each tower, we assess its vulnerability related to water stress, governance, hydropolitical tension and future climatic and socio-economic changes. We conclude that the most important water towers are also among the most vulnerable, and that climatic and socio-economic changes will affect them profoundly. This could negatively impact 1.9 billion people living in (0.3 billion) or directly downstream of (1.6 billion) mountainous areas. Immediate action is required to safeguard the future of the world's most important and vulnerable water towers.

The term 'water tower' is used to describe the water storage and supply that mountain ranges provide to sustain environmental and human water demands downstream[1,2]. Compared to its downstream area, a water tower (seasonally) generates higher runoff from rain as a result of orographic precipitation and delays the release of water by storing it in snow and glaciers (because of lower temperatures at high altitude) and lake reserves. Because of their buffering capacity, for instance by supplying glacier melt water during the hot and dry season, water towers provide a relatively constant water supply to downstream areas. We define a water tower unit (WTU; see Methods, Extended Data Fig. 1) as the intersection between major river basins[5] and a topographic mountain classification based on elevation and surface roughness[6]. Since water supply and demand are linked at the river basin scale, the basin is the basis for the WTU. One WTU can therefore contain multiple topographically different mountain ranges and we assume that it provides water

to the areas in the downstream river basin that are hydrologically connected to the WTU (Extended Data Fig. 1, Extended Data Table 1 and 2). Subsequently, we consider only cryospheric WTUs by imposing thresholds on satellite-derived snow-cover data[7] and a glacier inventory[8], because the buffering role of glaciers and snow and the delayed supply of melt water is a defining feature of water towers. Consequently, there are regions (for example, in Africa), which do contain mountain ranges, but because of their small snow and ice reserves they do not meet the WTU criteria. In total, we define 78 WTUs globally (see Methods), which are home to more than 250 million people. However, more than 1.6 billion people live in areas receiving water from WTUs, which is about 22% of the global population[9] (Fig. 1).

Water towers have an essential role in the Earth system and are particularly important in the global water cycle[1,2]. In addition to their water supply role, they provide a range of other services[10,11]. About 50% of the global biodiversity hotspots on the planet are located in mountain regions[12], they contain a third of the entire terrestrial species diversity[13], and are extraordinarily rich in plant diversity[14]. Moreover, mountain ecosystems provide key resources for human livelihoods, host important cultural and religious sites, and attract millions of tourists globally[6]. Economically, 4% and 18% of the global gross domestic product (GDP) is generated in WTUs and WTU-dependent basins respectively[15]. Furthermore, mountains are highly sensitive to climate change[3,4] and are warming faster than low-lying areas owing to elevation-dependent warming[16]. Climate change therefore threatens the entire mountain ecosystem. Worldwide, the vast majority of glaciers are losing mass[17], snow melt dynamics are being perturbed[18–21], and precipitation and evapotranspiration patterns are shifting, all leading to future changes in the timing and magnitude of mountain water availability[22]. Besides, the combination of cryosphere degradation and increases in climate extremes implies changing sediment loads affecting the quality of water supplied by mountains[23].

Not only are the world's water towers crucial to human and ecosystem survival, the steep terrain in combination with extreme climatic conditions, and in some regions seismic or volcanic activity, frequently triggers landslides, rock fall, debris flows, avalanches, glacier hazards and floods[24,25]. Since 2000, over 200,000 people have died in WTUs as a result of natural disasters[26]. Climate change, in combination with population growth, urbanization and economic and infrastructural developments, is likely to exacerbate the impact of natural hazards and further increase the vulnerability of these water towers[23,27–30].

QUANTIFYING IMPORTANCE OF WATER TOWERS

Consequently, there is a strong need for a consistent framework within which to assess and rank the importance and vulnerability of individual WTUs in order to guide global research, as well as conservation and policy-making efforts. Here we develop such a framework according to quantifiable indicators for both the water supply and demand sides of each WTU. Conceptually, a WTU is deemed to be important when its water resources (liquid or frozen) are plentiful relative to its downstream water availability and when its basin water demand is high and cannot be met by downstream water availability alone. Ideally, such an assessment would require a global-scale, high-resolution, fully coupled atmospheric–cryospheric–hydrological model that can resolve the interactions between extreme topography and the atmosphere, fully account for snow and ice dynamics, and incorporate anthropogenic interventions in the hydrological cycle. It would also require models that include socio-economic impacts on sectoral water demands and a spatially explicit attribution of water sources (for example, meltwater, groundwater, surface runoff) to water use. Although excellent progress has been made in specific regions and for specific sectors[31], at the global scale this is not yet feasible. We therefore derive indices covering relevant drivers for both the water supply and demand of a WTU's water budget (see Methods), which we combine to derive a water tower index (WTI).

The supply index (SI) is based on the average of four indicators that are quantified for each WTU: precipitation, snow cover, glacier ice storage and surface water (Fig. 2a, Extended Data Table 3, Supplementary Table 1 and Methods). If the precipitation in the WTU (Extended Data Fig. 3a) is high relative to the overall basin precipitation and if the inter-annual and intra-annual variation is low (that is, the supply is constant), a WTU scores highly on the precipitation indicator. If a WTU has persistent snow cover (Extended Data Fig. 3b) throughout the year and the snowpack shows lower inter-annual variation, this will result in a high snow indicator. Similarly, if the total glacier ice volume (Extended Data Fig. 4a) and glacier melt water yield in a WTU are high relative to the basin precipitation then a WTU has a high glacier ice storage indicator value. Finally, we assess the amount of water stored in lakes and reservoirs in a WTU (Extended Data Fig. 4b) compared to basin precipitation to derive a surface water indicator.

There is considerable variability in the power of WTUs to supply water. In Asia, the Tibetan Plateau has the highest ranking because of the large amounts of water stored in lakes, but a large part of the Tibetan Plateau is endorheic and its water resources are disconnected from the

downstream demand. The Indus WTU has an important water-supplying role with a balanced mix of precipitation, glaciers, snow and surface water. In Europe, the Arctic Ocean islands, Iceland and Scandinavia have extensive stocks of water stored in their WTUs. Iceland stands out with some of the thickest glaciers in the world and a glacier ice storage (about 1,027 km^3) that is 15 times as large as its total annual WTU precipitation (about 67 km^3). In South America, the mountain ranges (Extended Data Tables 1 and 2) supplying the Southern Chilean Pacific coast regions and La Puna Region are the most prominent water towers, because of large glacier ice reserves and high orographic precipitation rates and because of the large amount of water stored in lakes (in the La Puna region). The Northwest Territories and Nunavut, Fraser and the Pacific and Arctic coast are the key WTUs in North America. In the Northwest Territories and Nunavut the significance of the WTU is primarily driven by the abundance of glaciers, snow and surface water. However, the precipitation indicator value is low, meaning that mountain precipitation is low relative to the overall basin precipitation.

To derive a demand index (DI) for each WTU, we quantify the monthly water requirements to be supplied by the water towers to sustain the WTU basin's net sectoral water demand for irrigation, industrial (energy and manufacturing) and domestic purposes, and monthly natural water demand, relative to the total annual demand (Fig. 2b, Extended Data Table 4, Supplementary Table 1). Monthly sectoral water requirements are estimated by subtracting the monthly water availability downstream (ERA5 precipitation minus natural evapotranspiration[32]) from the monthly net demands[33]. The DI is the average of the four indicators (see Methods). Figure 2b demonstrates considerable variability, globally and within continents, in the demands that WTUs need to sustain. Irrigation water demands are the highest of the four demand types, and this is relatively consistent across the continents. The Asian river basins, specifically the heavily irrigated and densely populated basins such as the Indus, Amu Darya, Tigris, Ganges-Brahmaputra and Tarim, score more highly on the DI than other basins across the world and they score highly on each sectoral demand indicator. In those basins, the water required to close the gap between demand and downstream supply may also originate from (unsustainable) groundwater use[34,35]. However, in those cases, when there is a large water gap being (partly) closed by unsustainable groundwater pumping, the WTU water supply is critical both to meet the demand and to recharge the aquifers.

In Europe, the Volga and Ural in Russia show the highest DI values, including high values for the natural demand indicator, whereas the Negro basin has the highest DI in South America. In

North America a range of basins scores equally highly, but for different reasons. For example, the Mississippi–Missouri basin scores highly particularly because of a high natural demand indicator value, whereas the California basin scores highly on all four demand indicators.

Ultimately, the presence of mountain water resources, either as additional rain or stored in snow, ice or lakes, in conjunction with a high demand downstream, determines whether a WTU has an indispensable role (Extended Data Fig. 2). The WTI is the product of the SI and the DI, for which the values are subsequently normalized over the range of WTI values found for all 78 WTUs (Fig. 1, Supplementary Table 1). Globally, the upper Indus basin is the most critical water tower unit (WTI = 1.00 ± 0.03) with abundant water resources in the Karakoram, Hindu-Kush, Ladakh and Himalayan mountain ranges in combination with a densely populated and intensively irrigated downstream basin[22,36]. In North America, the Fraser and Columbia river basins are the most critical WTUs (WTI = 0.62 ± 0.07 and 0.58 ± 0.06, respectively). The Fraser basin is rich in surface water resources, and has a high natural water demand downstream, whereas the Columbia basin is rich in snow and glacier resources in combination with a high irrigation demand. In South America, the Cordillera Principal, the Cordillera Patagónica Sur and the Patagonian Andes are key WTUs in the supply of water to the South Atlantic and Pacific coastal regions and the Negro basin. In Europe, the Alps are the most relevant water-supplying mountain range, meeting the demands of the Rhône (WTI = 0.45 ± 0.07), Po (WTI = 0.39 ± 0.07) and Rhine (WTI = 0.32 ± 0.11) basins. We note that several WTUs that score highly on either the SI or the DI do not rank highly in the final WTI. For example, the Tibetan Plateau and Arctic Ocean islands WTUs score highly on the SI, but have the lowest scores on the DI, owing to low water demands (Fig. 2b). By contrast, the Sabarmati in Asia with a small portion of its water coming from the Himalayas has the highest DI, but a low SI.

VULNERABILITY OF THE WATER TOWERS

We assess the vulnerability of each WTU and show this for the five most important (that is, with highest WTI values) WTUs in Asia and Oceania, Europe, North America and South America (Fig. 3, Supplementary Table 2). For this analysis, we include the hydro-political tension[37], baseline water stress[38], government effectiveness[39], projected climate change[40], projected change in GDP[41], and projected population change[9] (see Methods). The highest-ranking WTUs of South America and Asia in particular are more vulnerable than those in North America and Europe. Strikingly, the Indus,

which is globally the most important water tower (Fig. 4), is also very vulnerable. The Indus is a transboundary basin with considerable hydro-political tension between its riparian countries Pakistan, India, China and Afghanistan. The population of approximately 206 million people in the basin in 2016 is projected to increase by 50% until 2050, and the basin's GDP is projected to encounter a nearly eightfold increase[41]. The temperature in the Indus WTU is projected to increase by 1.9 °C between 2000 and 2050, compared to 1.8 °C in the downstream section[40]. The average annual precipitation in the Indus WTU is projected to increase by 0.2%, compared to 1.4% downstream[40]. It is evident that, owing to the expected strong growth in population and economic development, the demand for fresh water will rise exponentially[42]. Combined with increased climate change pressure on the Indus headwaters, an already high baseline water stress and limited government effectiveness, it is uncertain whether the basin can fulfil its water tower role within its environmental boundaries. It is unlikely that the Indus WTU can sustain this pressure.

The Indus does not stand alone, however. Nearly all important WTUs in Asia are also highly vulnerable (Fig. 3). Most WTUs are transboundary, densely populated, heavily irrigated basins and their vulnerability is primarily driven by high population and economic growth rates and, in most cases, ineffective governance. Moreover, the Syr Darya, Amu Darya and Indus, in particular, are characterized by considerable hydro-political tension[37]. In most cases, downstream riparian states are dependent on mountain water resources provided by bordering upstream states to supply the competing irrigation, hydropower and domestic demands. In South America, the vulnerability is less than for the Asian WTUs, and the drivers are variable. On northern Chile's Pacific coast, the baseline water stress and a projected decrease in precipitation (−4.8%) cause the vulnerability, whereas population and economic growth render the La Puna region's WTU vulnerable. In North America, the vulnerabilities are related to population growth and temperature increase.

GLOBAL ASSETS WITH INCREASING IMPORTANCE

Planetary boundaries (for example, the CO_2 concentration, global freshwater use and biosphere integrity) are defined as thresholds within which humanity can safely function without abrupt large-scale changes to the environment[43]. Climate change and biosphere integrity have been identified as the core planetary boundaries with the potential to change the state of the Earth system should they be consistently transgressed for a prolonged period of time[44]. The global food system, in

particular, has been identified as a major pressure on the planetary boundaries[45]. Without targeted technological changes and mitigation measures, it is expected that the adverse environmental effects of the food system could increase by more than 50% by 2050 relative to 2010, thus crossing the planetary boundaries[45]. In relation to the planetary boundaries, water towers are of particular importance. They are highly vulnerable to climate change, a key water supply that sustains the major global food systems in the world and rich in biodiversity.

A clear implication is that vulnerability can be decreased with conservation, or increased with inefficient water use. This may seem logical and obvious, but it also means that the priorities for the most urgent action can be shifted as the nations of WTUs practice conservation or grow in an unsustainable way. Although irreversible changes in the buffering capacity of water towers are underway, conservation of the water towers in the broadest sense starts with the global task to mitigate further global climate warming leading to cryosphere degradation and its adverse effects on the water towers' buffering role. In a more local or regional context, water conservation is the one part of the equation that is under the control of an individual nation's part of a water tower system, calling for transboundary cooperation. Specific conservation can, for example, imply preserving the buffering capacity of mountain ranges in newly established protected areas, increasing the buffering capacity with reservoirs, and conservation of water by increasing water-use efficiency. Efficient use of scarce water resources can translate into improved wellbeing of people and increased economic and food security.

The vulnerability of these water towers in the future is controlled by the trajectory of change that a WTU and its associated downstream basin will follow. At the global scale we made a first-order assessment for a middle-of-the-road scenario both in terms of climate change and of socio-economic pathway (see Methods). However, it is important to acknowledge that the future pathways are extremely precarious and the outcomes diverging and uncertain. A recent assessment for the Hindu-Kush Himalayan region concluded that there is no single likely future: the region may run downhill, may do business as usual or it may advance to prosperity[46]. Each of those future pathways will result in systematically different demands for water and may cross the planetary boundaries in varying degrees and this will probably hold for most WTUs, but those in Asia and South America in particular.

Mountains are also an essential resource in the context of the United Nations' Sustainable Development Goals (SDGs) that have been targeted towards the year 2030[47]. Mountains play a key

part in achieving the SDGs for water (SDG 6), food (SDG 2) and energy (SDG 7). Given the projected change in climate and socioeconomic development in mountain-dependent basins, it is evident that if the SDGs are to be achieved the water resources of the water towers need to be harnessed within safe environmental limits.

We therefore make three essential recommendations. First, mountain regions must be recognized as a global asset of the Earth system. Second, it must be acknowledged that vulnerability of the world's water towers is driven both by socio-economic factors and climate change. Third, we must develop international, mountain-specific conservation and climate-change adaptation policies (such as national parks, pollutants control, emission reductions, erosion control and dam regulations) that safeguard the mountain ecosystems and mountain people and simultaneously ensure water, food and energy security of the millions of people downstream.

Received 27 May 2019; accepted 11 November 2019

Published online 9 December 2019.

REFERENCES

1. Viviroli, D., Dürr, H. H., Messerli, B., Meybeck, M. & Weingartner, R. Mountains of the world, water towers for humanity: typology, mapping, and global significance. Wat. Resour. Res. 43, 1–13 (2007).

2. Immerzeel, W. W., Van Beek, L. P. & Bierkens, M. F. P. Climate change will affect the Asian water towers. Science 328, 1382–1385 (2010).

3. Viviroli, D. et al. Climate change and mountain water resources: overview and recommendations for research, management and policy. Hydrol. Earth Syst. Sci. 15, 471–504 (2011).

4. IPCC Special Report on the Ocean and Cryosphere in a Changing Climate https://www.ipcc.ch/report/srocc/ (2019)

5. Lehner, B., Verdin, K. & Jarvis, A. New global hydrography derived from spaceborne elevation data. Eos 89, 93–104 (2008).

6. Körner, C. et al. A global inventory of mountains for bio-geographical applications. Alp. Bot. 127, 1–15 (2017).

7. Hall, D. K. & Riggs, G. A. MODIS/Terra Snow Cover Monthly L3 Global 0.05Deg CMG Version 6 (2015). http://10.5067/MODIS/MOD10CM.006

8. Pfeffer, W. et al. The Randolph Glacier Inventory: a globally complete inventory of glaciers. J. Glaciol. 60, 537–552 (2014).

9. Klein Goldewijk, K., Beusen, A., Van Drecht, G. & De Vos, M. The HYDE 3.1 spatially explicit database of human-induced global land-use change over the past 12,000 years. Glob. Ecol. Biogeogr. 20, 73–86 (2011).

10. Xiao, C.-D., Wang, S. J. & Qin, D. H. A preliminary study of cryosphere service function and value evaluation. Adv. Clim. Chang. Res. 6, 181–187 (2015).

11. Wang, X., Liu, S. W. & Zhang, J. L. A new look at roles of the cryosphere in sustainable development. Adv. Clim. Chang. Res. 10, 124–131 (2019).

12. Chape, S., Spalding, M. D. & Jenkins, M. D. The World's Protected Areas (UNEP-World Conservation Monitoring Centre, 2008).

13. Körner, C. & Paulsen, J. A world-wide study of high altitude treeline temperatures. J. Biogeogr. 31, 713–732 (2004).

14. Körner, C., Paulsen, J. & Spehn, E. M. A definition of mountains and their bioclimatic belts for global comparisons of biodiversity data. Alp. Bot. 121, 73–78 (2011).

15. Nordhaus, W. D. Geography and macroeconomics: new data and new findings. (2006)

16. Pepin, N. et al. Elevation-dependent warming in mountain regions of the world. Nat. Clim. Chang. 5, 424–430 (2015).

17. Zemp, M. et al. Global glacier mass changes and their contributions to sea-level rise from 1961 to 2016. Nature 568, 382–386 (2019).

18. Hammond, J. C., Saavedra, F. A. & Kampf, S. K. Global snow zone maps and trends in snow persistence 2001–2016. Int. J. Climatol. 38, 4369–4383 (2018).

19. Bormann, K. J., Brown, R. D., Derksen, C. & Painter, T. H. Estimating snow-cover trends from space. Nat. Clim. Chang. 8, 924–928 (2018).

20. Sarangi, C. et al. Impact of light-absorbing particles on snow albedo darkening and associated radiative forcing over High Mountain Asia: high resolution WRF-Chem modeling and new satellite observations. Atmos. Chem. Phys. Discuss. http://doi.org/10.5194/acp-2018–979 (2018).

21. Painter, T. H. et al. Impact of disturbed desert soils on duration of mountain snow cover. Geophys. Res. Lett. 34, L12502 (2007).

22. Lutz, A. F., Immerzeel, W. W., Shrestha, A. B. & Bierkens, M. F. P. Consistent increase in High Asia's runoff due to increasing glacier melt and precipitation. Nat. Clim. Chang. 4, 587–592 (2014).

23. Huss, M. et al. Toward mountains without permanent snow and ice. Earth. Future 5, 418–435 (2017).

24. Kargel, J. S. S. et al. Geomorphic and geologic controls of geohazards induced by Nepal's 2015 Gorkha earthquake. Science 351, aac8353 (2016).

25. Kirschbaum, D. et al. The state of remote sensing capabilities of cascading hazards over high mountain Asia. Front. Earth Sci. https://doi.org/10.3389/feart.2019.00197 (2019).

26. Guha-Sapir, D., Below, R. & Hoyois, P. EM-DAT: International Disaster Database (2019).

27. Mal, S. Climate Change, Extreme Events and Disaster Risk Reduction (Springer, 2018).

28. Mann, M. E. et al. Influence of anthropogenic climate change on planetary wave resonance and extreme weather events. Sci. Rep. 7, 45242 (2017).

29. Fischer, E. M. & Knutti, R. Anthropogenic contribution to global occurrence of heavy-precipitation and high-temperature extremes. Nat. Clim. Chang. 5, 560–564 (2015).

30. Haeberli, W., Schaub, Y. & Huggel, C. Increasing risks related to landslides from degrading permafrost into new lakes in de-glaciating mountain ranges. Geomorphology 293, 405–417 (2017).

31. Biemans, H. et al. Importance of snow and glacier meltwater for agriculture on the Indo-Gangetic Plain. Nat. Sustain. 2, 594–601 (2019).

32. C3S. ERA5: Fifth generation of ECMWF atmospheric reanalyses of the global climate. (2017).

33. Wada, Y., De Graaf, I. E. M. & van Beek, L. P. H. High-resolution modeling of human and climate impacts on global water resources. J. Adv. Model. Earth Syst. 8, 735–763 (2016).

34. Wada, Y. et al. Global depletion of groundwater resources. Geophys. Res. Lett. 37, https://doi.org/10.1029/2010GL044571 (2010).

35. Wada, Y., Van Beek, L. P. H. & Bierkens, M. F. P. Nonsustainable groundwater sustaining irrigation: a global assessment. Wat. Resour. Res. 48, https://doi.org/10.1029/2011WR010562 (2012).

36. Immerzeel, W. W. & Bierkens, M. F. P. Asia's water balance. Nat. Geosci. 5, 841–842 (2012).

37. De Stefano, L., Petersen-Perlman, J. D., Sproles, E. A., Eynard, J. & Wolf, A. T. Assessment of transboundary river basins for potential hydro-political tensions. Glob. Environ. Change 45, 35–46 (2017).

38. Hofste, R. W. et al. Aqueduct 3.0: Updated Decision-Relevant Global Water Risk Indicators. Technical Note (2019).

39. Kaufmann, D., Kraay, A. & Mastruzzi, M. The Worldwide Governance Indicators. Methodology and Analytical Issues. Policy Research Working Paper 5430 (2010).

40. Taylor, K. E., Stouffer, R. J. & Meehl, G. A. An overview of CMIP5 and the experiment design. Bull. Am. Meteorol. Soc. 93, 485–498 (2012).

41. Murakami, D. & Yamagata, Y. Estimation of gridded population and GDP scenarios with spatially explicit statistical downscaling. Preprint at https://arxiv.org/abs/1610.09041 (2016).

42. Wijngaard, R. R. et al. Climate change vs. socio-economic development: understanding the South-Asian water gap. Hydrol. Earth Syst. Sci. 22, 6297–6321 (2018).

43. Rockström, J. et al. Planetary boundaries: exploring the safe operating space for humanity. Ecol. Soc. 14, 32 (2009).

44. Jaramillo, F. & Destouni, G. Comment on “Planetary boundaries: Guiding human development on a changing planet”. Science 348, 1217 (2015).

45. Springmann, M. et al. Options for keeping the food system within environmental limits. Nature 562, 519–525 (2018).

46. Roy, J. et al. Exploring futures of the Hindu Kush Himalaya: scenarios and pathways. In The Hindu Kush Himalaya Assessment: Mountains, Climate Change, Sustainability and People (eds Wester, P., Mishra, A., Mukherji, A. & Shrestha, A. B.) 99–125 (Springer International Publishing, 2019).

47. United Nations. Transforming Our World: The 2030 Agenda For Sustainable Development. A/RES/70/1 (2015).

FIGURES

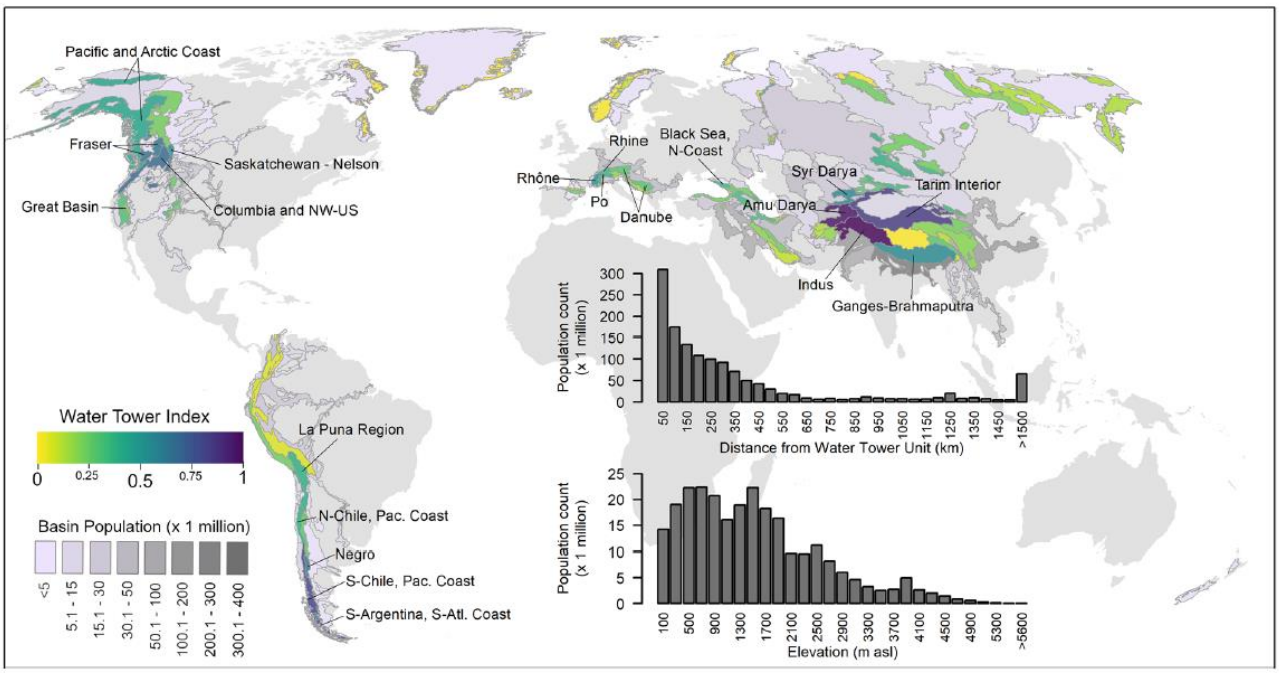

Fig. 1 The WTI, the population in WTUs and their downstream basins. The WTI, derived from the SI and the DI, is shown for all 78 WTUs, in combination with the shaded total population in all WTU-dependent river basins. Labels indicate the five water towers with the highest WTI value per continent. The insets show the number of people living in WTUs as a function of elevation and of the downstream population's proximity to the WTUs[9].

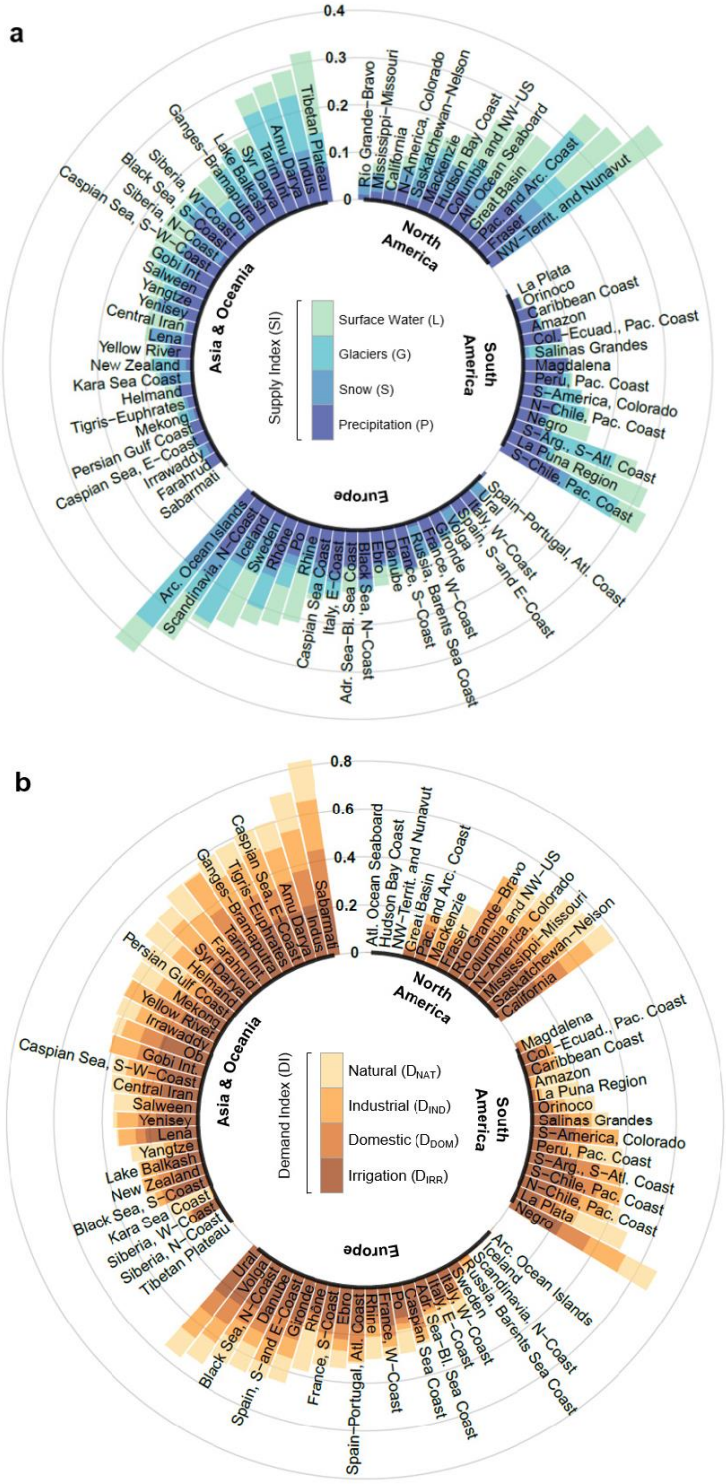

Fig. 2 The SI and DI. a, **b**, The SI (**a**) and the DI (**b**) of each WTU grouped by continent and ordered by SI or DI value, respectively. Increasing radially, the stacked bars show the four indicator values for surface water (*L*), glacier (*G*), snow (*S*) and precipitation (*P*), respectively. In b, increasing radially, the stacked bars show the four indicator values for natural (D_{NAT}), industrial (D_{IND}),

domestic (D_{DOM}) and irrigation demands (D_{IRR}), respectively. Calculation details of the indicators and index of the indices are provided in Extended Data Tables 3 and 4.

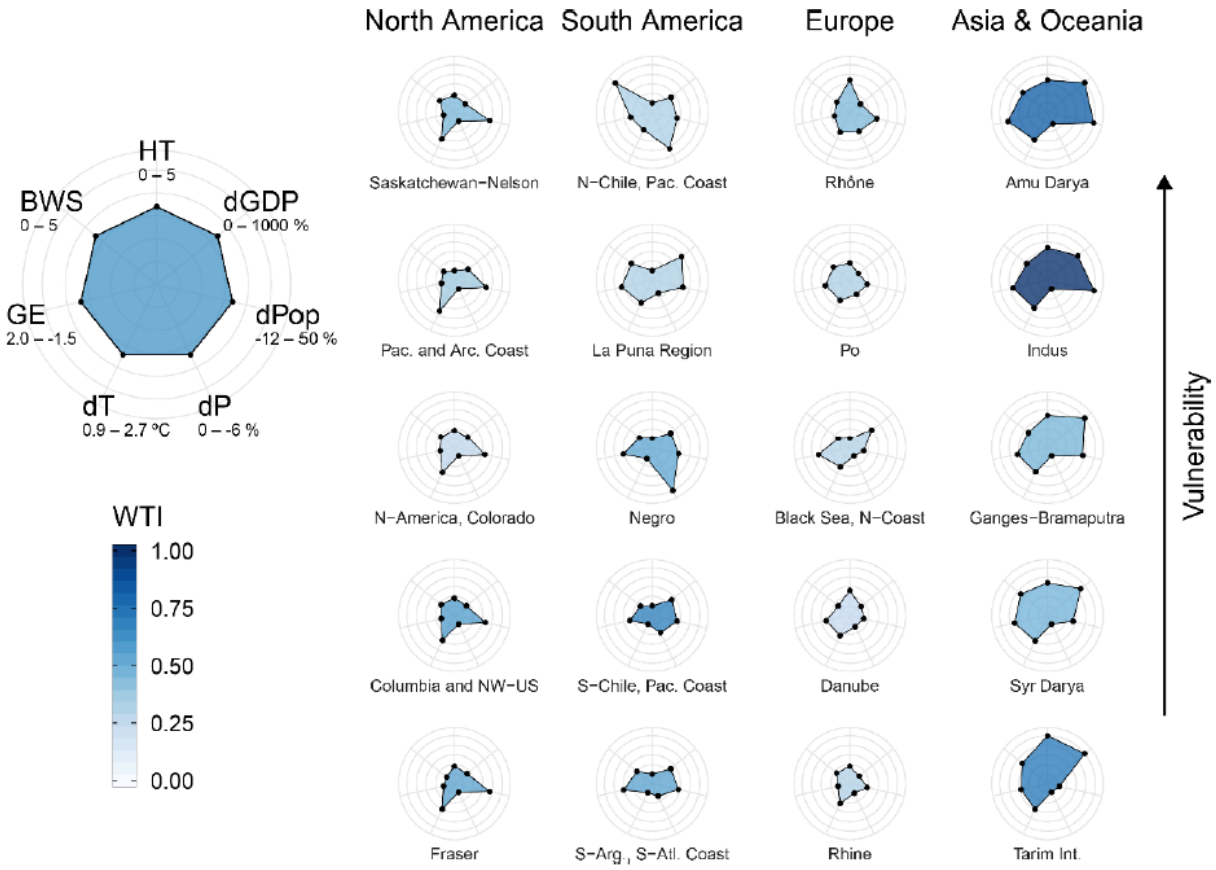

Fig. 3 The vulnerability and projected change of the top five WTUs of each continent. The total vulnerability (indicated by larger polygons), and projected change indicators of the five most important WTUs on each continent. BWS is the baseline water stress indicator of the basin[38]; GE is an indicator for government effectiveness in the basin[39]; HT is hydro-political tension[37]; dGDP[41] and dPop[9] are the projected changes in gross domestic product and population between 2000 and 2050, according to Shared Socioeconomic Pathway 2 (SSP2); dP[40] and dT[40] are the projected precipitation and temperature changes between 2000 and 2050 according to the CMIP5 multi-model ensemble mean for Representative Concentration Pathway (RCP) 4.5. WTUs are ranked by vulnerability (highest vulnerability on top); colour filling indicates the WTU's WTI value. See Methods for calculation details.

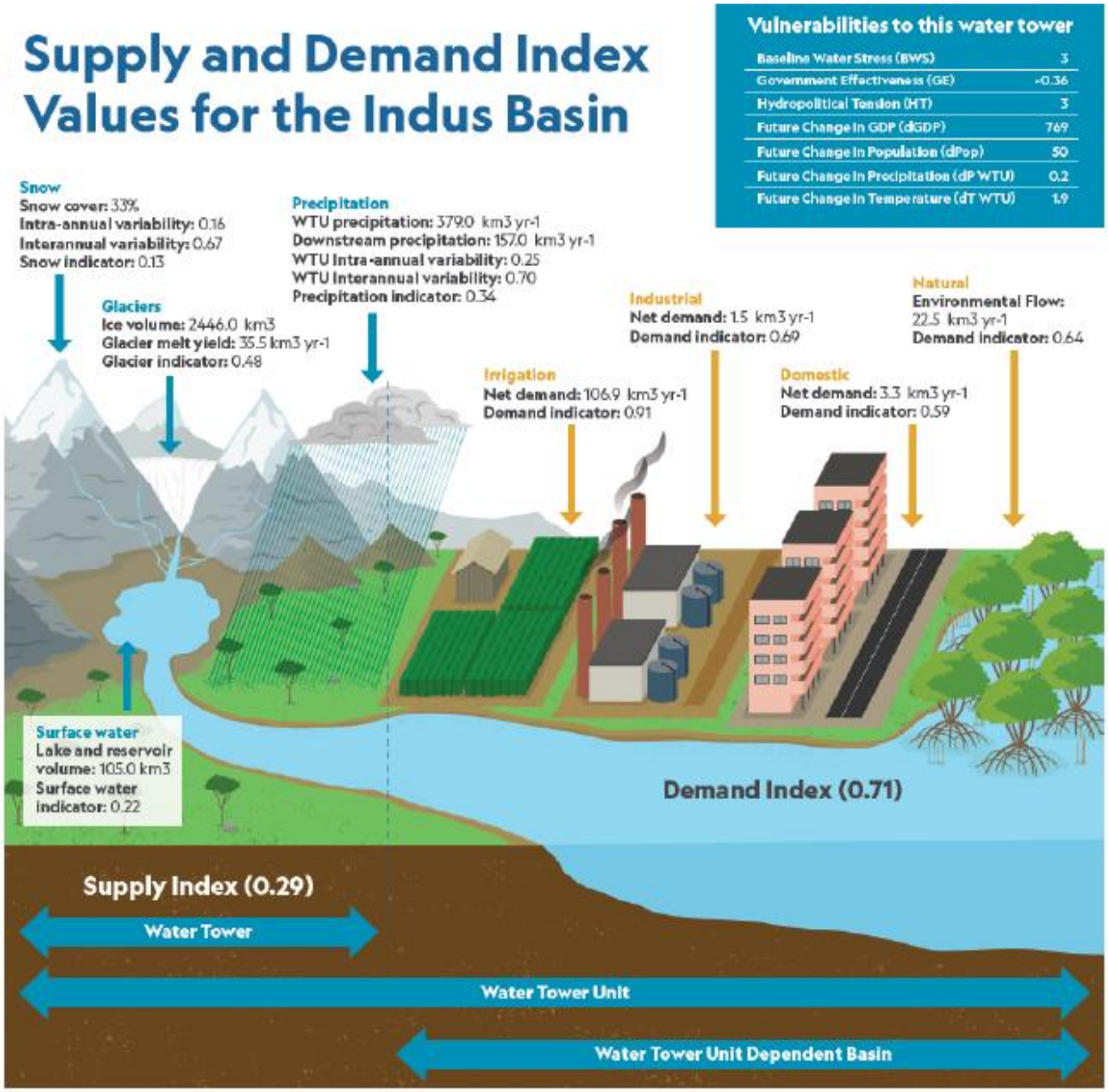

Fig. 4 WTI and vulnerabilities of the Indus basin. a, The supply and demand indicators. **b**, The vulnerabilities. See Methods for details on the supply and demand indicators and the meaning of the vulnerability ranges. S_T, snow cover; S_{MV}, intra-annual snow variability; S_{YV}, inter-annual snow variability. G_S, glacier ice volume; G_M, glacier melt yield. P_T, WTU precipitation; P_{BAS}, downstream precipitation; P_{MV}, WTU intra-annual precipitation variability; P_{YV}, WTU inter-annual precipitation variability. $D_{ind,Y}$, net industrial demand; D_{IND}, industrial demand indicator. $D_{NAT,Y}$, net natural demand; D_{NAT}, natural demand indicator. $D_{DOM,Y}$, net domestic demand; D_{DOM}, domestic demand indicator. $D_{IRR,Y}$, net irrigation demand; D_{IRR}, irrigation demand indicator.

METHODS

Delineation of WTUs

In this study, we define a WTU as the intersection of major river basins[5] and a topographic mountain classification based on elevation and surface roughness developed in the framework of the Global Mountain Biodiversity Assessment (GMBA)[6]. Although other similar mountain classification datasets exist[1] that are also based on a combination of elevation and surface roughness, we use the GMBA classification (version 1.2) because topographical names of mountain ranges have been assigned to each of the mountain regions classified. The original GMBA inventory contains 1,048 mountain regions worldwide. We make a subset of this dataset by imposing minimum thresholds for glacier area, glacier ice volume and snow persistence. We retain those mountain regions which have an ice volume larger than 0.1 km^3 (ref. [48]) or an average annual areal snow persistence larger than 10%[7]. After imposing these thresholds, 174 mountain regions remain. We intersect those regions with the major river basins and dissolve the result based on major river basin ID; that is, all selected GMBA regions within a basin are grouped as a single WTU (Extended Data Fig. 1, Extended Data Table 1, Extended Data Table 2). The final WTU delineation contains 78 units (Extended Data Fig. 1). For each WTU we also define the downstream area that directly depends on the WTU using the river sub-basin delineation[5], and we specify which mountain ranges are part of the WTU (Extended Data Fig. 1, Extended Data Table 1, Extended Data Table 2). This dependent downstream area is smaller than the total downstream basin because not every downstream sub-basin is hydrologically connected to the WTU. To this end we start at the WTU and iteratively select each connected downstream sub-basin until the basin outlet, or lowest sub-basin in case of an endorheic system, is reached (Extended Data Fig. 1).

Quantifying the WTI

We combine an SI and a DI into a WTI with which to rank WTUs. All grid calculations are performed at 0.05° resolution.

The SI (see Extended Data Table 3 for all equations) is based on indicators for precipitation, snow cover, glaciers and surface water storage. For the precipitation indicator, the 2019 released ERA5 reanalysis dataset is used[32]. As sub-indicators, we first compute the total annual average (2001–2017) WTU precipitation (Extended Data Fig. 3a) relative to the overall basin precipitation (PT). We

then include the inter-annual variation in WTU precipitation (PYV) and the intra-annual monthly WTU variation (PMV) based on the 2001–2017 time series. We combine these three sub-indicators into a precipitation indicator (P), giving the variation (PYV and PMV) the same weight as PT. The underlying assumption of including the variation is that if the variation is low, the WTU will provide a constant flow of water to the downstream basin, and therefore it is a more important WTU. For the snow cover indicator, we use the MODIS MOD10CM1 product[7]. We derive an average annual snow cover (ST) in each WTU for the 2001–2017 period (Extended Data Fig. 3b). Here too, we derive both an inter-annual (SYV) and intra-annual (SMV) variation in snow cover, and using the same rationale as for the precipitation indicator, we combine the average snow persistence with the variation to derive a final snow indicator (S). For the glacier indicator, we compute the glacier ice volume in a WTU48 (Extended Data Fig. 4a) relative to the average annual WTU precipitation (GS). We also compute the annual glacier melt water flux relative to the WTU precipitation on non-glacierized terrain (GM). We estimate the glacier melt water flux as the sum of the on-glacier precipitation and the mass balance per WTU. The WTU mass balance is based on the area-weighted average annual mass balance from all geodetic and direct mass balance measurements made available by the World Glacier Monitoring Service49. However, if there are fewer than ten glaciers with data available within a WTU then we use the regional average[17]. We sum GS and GM to derive a final glacier indicator (G). For the surface water indicator (L), we compute the total volume of water that is stored in lakes and reservoirs in a WTU50 (Extended Data Fig. 4b) relative to the average annual WTU precipitation. The supply indicator is the average of P, S, G and L.

The DI is based on net human water demands for domestic, industrial and irrigation purposes[33], and natural demand (see Extended Data Table 4 for all equations, Extended Data Fig. 5, Extended Data Fig. 6). Since the natural demand, defined as the minimum river flow required to sustain the ecosystem, is not readily available, we estimate it with the environmental flow requirement computed with the 90th-percentile exceedance value of the natural flow[33,51,52]. First, the average monthly sectoral demands are computed based on a 2001–2014 time series ($D_{DOM,m}$, $D_{IRR,m}$, $D_{IND,m}$, $D_{NAT,m}$). Part of each sectoral demand can potentially be met by downstream water availability that does not have its origin in the mountains. For each grid cell with a positive demand we therefore compute the average monthly water availability ($WA_{DOM,m}$, $WA_{IRR,m}$, $WA_{IND,m}$, $WA_{NAT,m}$; see Extended Data Table 4) as the precipitation minus the actual natural evapotranspiration[32]. We subtract this amount from the average monthly sectoral water demands as an estimate for the

monthly demand that needs to be met by other sources, including the WTUs. We assume that the entire water deficit has to be provided by the WTU, although other water sources, such as groundwater[51], can also be important. We acknowledge that the global scale of our assessment also prevents us from fully taking into account the distribution and allocation of water within different portions of our spatial units of calculation. Finally, we aggregate these monthly net demands to be sustained by the WTU over all months and we divide it by the total annual sectoral demand to get four demand indicators (D_{DOM}, D_{IND}, D_{IRR}, D_{NAT}). The DI is the average of the indicators D_{DOM}, D_{IND}, D_{IRR} and D_{NAT}.

The final WTI is the product of SI and DI, for which the values are subsequently normalized over the range of WTI values found for all 78 WTUs. By using a multiplicative approach, we ensure that a WTU only ranks highly when it has considerable water resources (either as precipitation, glacier ice, snow and surface water or a combination) in the mountains, and the demand for those resources downstream is likewise high (Extended Data Fig. 2).

Uncertainty

It is acknowledged that the SI, DI and WTI are based on partly arbitrary choices of indicators and sub-indicators. In our assessment we have assigned an equal weight to each of the indicators constituting SI and DI. To account for uncertainty in the weight of each indicator in the WTI calculation we have performed a sensitivity analysis in which we randomly vary the weights of each of the eight indicators that constitute the SI and DI and assess the impact on the WTI ranking of the WTUs. We assume that the weight of each indicator is uniformly distributed and can be a maximum of three times as high or low as another indicator, and we assess through a 10,000-member Monte Carlo analysis how sensitive the rank of the WTU is as a result of this uncertainty. The analysis shows that the top and bottom of the ranking are robust and only limited shifts in the ranking occur (<5 positions). However, the middle part of the ranking is more sensitive to the weights of the indicators and there is a considerable number of WTUs where, in more than 25% of the total runs, the rank changes more than 5 positions.

In addition, we also include a 1,000-member Monte Carlo analysis to assess the propagation of uncertainty in the datasets used in the WTI calculation. For each input dataset we estimate a standard deviation and assuming a normally distributed error we sample from the distribution to

assess how the input data uncertainty affects the WTI value (Supplementary Table 1) and WTU ranking (Extended Data Fig. 7). For precipitation we compute the standard deviation per WTU and per downstream basin based on nine different precipitation datasets (CRU bias-corrected with ERA-Interim, CRU TS2.1 downscaled with ERA-40, CRU TS3.21 downscaled with ERA-40, CRU TS3.21 downscaled with ERA-Interim, WFDEI, NCEP-NCAR Reanalysis, WATCH, WATCH corrected with GPCC, and ERA5)[32,53–59]. For evapotranspiration we take a similar approach using four different datasets (ERA-Interim, GLEAM, MERRA-2, PCR-GLOBWB forced with ERA-Interim, and ERA5)[32,54,60–62]. Values for snow persistence, ice volumes, glacier mass balance, and the domestic, industrial and irrigation water demands are derived from the literature[17,48,63–65]. For the uncertainty in lake and reservoir volume we assume a standard deviation of 10% and we keep the environmental flow requirement constant. The ranking is also sensitive to input data uncertainty; however, the ranking is robust, in particular in the top 20 places of the ranking where only limited shifts in positions occur. Here, too, most shifts are observed in the middle part of the ranking.

Assessing vulnerabilities

For the WTUs, we assess the vulnerability of their role as water tower based on three static indicators for water stress, government effectiveness and the potential for hydro-political tension in case of transboundary basins (Supplementary Table 2). In addition, we include four change indicators: the projected change in temperature, precipitation, population and gross domestic product between 2000 and 2050. In all cases we use the ensemble mean RCP4.5 climate change scenario[66] in combination with the SSP2 shared socio-economic pathway[67] as a middle-of-the-road scenario, both in terms of economic development and associated climate change (Supplementary Table 2). We scale the different vulnerability indicators between 0 (minimum vulnerability) and 1 (maximum vulnerability) considering the thresholds defined below.

For water stress, we use the baseline water stress (BWS) indicator[38]. BWS measures the ratio of total water withdrawals to the available renewable surface and groundwater supplies; higher values indicate more competition among users. The index value is derived from an ordinary least-squares regression fitted through raw monthly water-stress values for 1960–2014, taking the fitted BWS value for 2014[38]. We compute the area-averaged BWS for all WTUs, including their downstream dependent areas and scale between 0 and 5, which is the range of the BWS scale in the cited study. High BWS is associated with high vulnerability and low BWS is associated with low

vulnerability. Since no global dataset for water management capacity is available at the global scale we validated the indicators gross domestic product (GDP)[68], human development index (HDI)[68] and government effectiveness (GE)[39] as proxies for water management capacity, which is available for selected mountainous basins only[3]. GE shows the best correlation with water management capacity in the selection of basins, and we calculate the area-averaged value for each WTU including its downstream dependent area. We scale between −1.5 and 2.0, which are the minimum and maximum values found for the WTUs. A low value for GE implies high vulnerability whereas a high value for GE indicates low vulnerability. Lastly, all transboundary basins are assessed on the risk for potential hydro-political tensions based on a global mapping of basins that are ill-equipped to deal with transboundary disputes triggered by the construction of new dams and diversions[37]. We compute the WTU basin aggregated score provided by the cited study and the range of the original scale in the cited study (0 to 5) is used to scale between minimum and maximum.

For each WTU we compute a projected multi-model ensemble mean change in precipitation (measured as a percentage) and temperature (measured in kelvin) between 2000 and 2050 for RCP4.5 for 35 different CMIP5 climate models[40]. For projected changes in temperature the scores for the individual WTUs are linearly scaled between 0 and 1 for the full range of projected temperature increases of all WTUs. For precipitation projections, only decreases in precipitation are assumed to contribute to vulnerability (that is, projections of increases in precipitation and unchanged precipitation are classified as minimum vulnerability). The scores for the individual WTUs are scaled linearly between 0 and 1, where 0 indicates unchanged or increasing precipitation and 1 indicates the largest precipitation decrease projected for all 78 WTUs. The projected population change between 2016 and 2050 for SSP2 is derived from the HYDE database[9] and the relative increase for each of the WTU basins is computed. All WTUs are scaled between a growth of 0% and a maximum of 50%, that is, if the projected population growth is more than 50%, a WTU has maximum vulnerability. The relative increase in GDP between 2000 and 2050 is computed per WTU basin, with the assumption that a strong projected increase in GDP is indicative of a strong growth in water demand. Data for the SSP2 shared socio-economic pathway are used[41]. All WTU basins are scaled between the minimum and the maximum, which is capped by a growth rate of 1000%.

We assess indicators of various nature for vulnerability and future changes. To assess a complete vulnerability based on this set of indicators is challenging and requires knowledge of the

weights of the individual indicators in assessing the total vulnerability for each WTU. The caveat is made that we consider a middle-of-the-road scenario both in terms of projected climate change and socio-economic development as a first-order assessment. The future development pathway in most WTUs, in particular in Asia and South America, is uncertain and highly diverging and depends on the global economy, regional growth rates and geopolitical tensions, which are difficult to project or quantify. In addition, a satisfactory representation of mountainous climate in General Circulation Models is difficult, leading to large uncertainty in particular for future precipitation projections.

In our study we assess impacts-driven vulnerability, where vulnerability is defined in direct proportion to the magnitude of hydrological change. However, we note that recent work on the human dimensions of climate change have demonstrated that vulnerability emerges from the interaction of both environmental and social dynamics in specific contexts[69,70].

Data availability

The data generated to support the findings of this study are available in an online data repository at zenodo.org with doi:10.5281/zenodo.3521933. **https://doi.org/10.5281/zenodo.3521933.** Third party data used in this study are available as follows. Hydrological basin boundaries[5] used in this study are available online at http://www.fao.org/nr/water/aquamaps/. Mountain definition data[6] used in this study are available online at https://ilias.unibe.ch/goto_ilias3_unibe_file_1047348.html. Precipitation and evaporation data used in this study[32] are available online at https://cds.climate.copernicus.eu. Snow cover data used in this study[7] are available online at https://nsidc.org/data/mod10cm. Glacier volume data[48] used in this study are available online at https://doi.org/10.3929/ethz-b-000315707. Glacier mass balance data[17,71] are available online at https://wgms.ch/. Lake and reservoir storage data[50] used in this study are available online at https://www.hydrosheds.org/pages/hydrolakes. Water demand data used in this study are available upon request from Y.W. (wada@iiasa.ac.at). BWS data[38] used in this study are available online at https://www.wri.org/aqueduct. GE data[39] used in this study are available online at https://info.worldbank.org/governance/wgi/#home. Data on hydro-political tensions for transboundary river basins[37] used in this study are available online at https://transboundarywaters.science.oregonstate.edu/content/transboundary-freshwater-spatial-database. Data for future projections of population count[9] used in this study are available online at

ftp://ftp.pbl.nl/hyde/SSPs/SSP2/zip/. Data for future projections of GDP[41] used in this study are available online at http://www.cger.nies.go.jp/gcp/population-and-gdp.html. Data for future projections of temperature and precipitation[40] used in this study are available online at https://climexp.knmi.nl.

Code availability

The code developed for the WTI calculations performed for this study are publicly available in a Github repository at https://github.com/mountainhydrology/pub_ngs-watertowers.

References

48. Farinotti, D. et al. A consensus estimate for the ice thickness distribution of all glaciers on Earth. Nat. Geosci. 12, 168–173 (2019).

49. World Glacier Monitoring Service Fluctuations of Glaciers (FoG) Database http://doi.org/10.5904/wgms-fog-2018-06 (2018).

50. Messager, M. L., Lehner, B., Grill, G., Nedeva, I. & Schmitt, O. Estimating the volume and age of water stored in global lakes using a geo-statistical approach. Nat. Commun. 7, 13603 (2016).

51. Gleeson, T., Wada, Y., Bierkens, M. F. P. & Van Beek, L. P. H. Water balance of global aquifers revealed by groundwater footprint. Nature 488, 197–200 (2012).

52. Smakhtin, V., Revenga, C. & Döll, P. A pilot global assessment of environmental water requirements and scarcity. Water Int. 29, 307–317 (2004).

53. Harris, I., Jones, P. D., Osborn, T. J. & Lister, D. H. Updated high-resolution grids of monthly climatic observations—the CRU TS3.10 dataset. Int. J. Climatol. http://doi.org/10.1002/joc.3711 (2013).

54. Dee, D. P. et al. The ERA-Interim reanalysis: configuration and performance of the data assimilation system. Q. J. R. Meteorol. Soc. 137, 553–597 (2011).

5. Weedon, G. P. et al. The WFDEI meteorological forcing data set: WATCH Forcing Data methodology applied to ERA-Interim reanalysis data. Wat. Resour. Res. 50, 7505–7514 (2014).

56. Weedon, G. P. et al. Creation of the WATCH Forcing Data and its use to assess global and regional reference crop evaporation over land during the twentieth century. J. Hydrometeorol. 12, 823–848 (2011).

57. Schneider, U. et al. GPCC's new land surface precipitation climatology based on quality-controlled in situ data and its role in quantifying the global water cycle. Theor. Appl. Climatol. 115, 15–40 (2014).
58. Uppala, S. M. et al. The ERA-40 re-analysis. Q. J. R. Meteorol. Soc. 131, 2961–3012 (2005).
59. Kalnay, E. et al. The NCEP/NCAR 40-Year Reanalysis Project. Bull. Am. Meteorol. Soc. 77, 437–471 (1996).
60. Martens, B. et al. GLEAM v3: Satellite-based land evaporation and root-zone soil moisture. Geosci. Model Dev. 10, 1903–1925 (2017).
61. Rienecker, M. M. et al. MERRA: NASA's modern-era retrospective analysis for research and applications. J. Clim. 24, 3624–3648 (2011).
62. Sutanudjaja, E. H. et al. PCR-GLOBWB 2: a 5 arcmin global hydrological and water resources model. Geosci. Model Dev. 11, 2429–2453 (2018).
63. Riggs, G. A., Hall, D. K. & Román, M. O. Overview of NASA's MODIS and VIIRS Snow-Cover Earth System Data Records. Earth Syst. Sci. Data Discuss. http://doi.org/10.5194/essd-2017-25 (2017).
64. Wada, Y. et al. Modeling global water use for the 21st century: the Water Futures and Solutions (WFaS) initiative and its approaches. Geosci. Model Dev. 9, 175–222 (2016).
65. Wada, Y. et al. Multimodel projections and uncertainties of irrigation water demand under climate change. Geophys. Res. Lett. 40, 4626–4632 (2013).
66. van Vuuren, D. P. et al. The representative concentration pathways: an overview. Clim. Change 109, 5–31 (2011).
67. O'Neill, B. C. et al. The roads ahead: narratives for shared socioeconomic pathways describing world futures in the 21st century. Glob. Environ. Change 42, 169–180 (2017).
68. Kummu, M., Taka, M. & Guillaume, J. H. A. Gridded global datasets for gross domestic product and human development index over 1990-2015. Sci. Data 5, 180004 (2018).
69. McDowell, G. et al. Adaptation action and research in glaciated mountain systems: Are they enough to meet the challenge of climate change? Glob. Environ. Change 54, 19–30 (2019).
70. Conway, D. et al. The need for bottom-up assessments of climate risks and adaptation in climate-sensitive regions. Nat. Clim. Chang. 9, 503–511 (2019).
71. Zemp, M. et al. WGMS (2017): Global Glacier Change Bulletin No. 2 (2014-2015). (2017).

Acknowledgements This project was funded as part of the National Geographic Society and Rolex Partnership to Support a Perpetual Planet. We are grateful to the Strategic Priority Research Program of the Chinese Academy of Sciences for their support, to D. Farinotti for providing the data on glacier volume, and to N. Wanders for providing precipitation datasets used in the uncertainty analysis.

Author contributions W.W.I. and A.F.L. contributed equally to the study; they designed the study, performed the analysis, prepared figures and tables and drafted the manuscript. P.D.A.K. contributed to the data analysis and prepared Fig. 3. Y.W. provided the dataset used to calculate demand indicators. S.B., S.H., A.B. and A.C.E contributed to the design of the index and analysis methods. All authors contributed to developing the theory and conception of the study by providing regional (M.A., A.F. and P.P. for the Andes; T.B., U.H., P.D.A.K., A.V.K., P.M., S.N., F.P., A.B.S., A.S., C.X. and T.Y. for High Mountain Asia; T.B., A.E., F.P. and D.V. for the Alps; and S.R., T.H.P., J.S.K. and M.K. for North America) or subject-specific expertise (B.J.D., J.S.K., A.B.S., P.P., A.S. and S.R. for glacial volume; U.H., M.K. and F.P. for meltwater discharge; H.B., A.F. and Y.W. on irrigation demand; T.B., A.C.E., J.S.K. and A.V.K. for glacial lakes; M.F. and T.H.P. for global snow cover, P.D.A.K. for volume ice loss; A.F., P.M., A.S. and T.Y. for climatology; S.N. and S.R. for hydrology; M.K., A.B.S. and D.V. for water demand, conflicts and vulnerability; H.R. for preferential flow; S.R. for glacier accumulation mass loss and its effects on downstream populations; D.V. for water management capacity; C.X. for global cryospheric functions and processes; and Y.W. for environmental flow requirements). All authors discussed and provided feedback on the manuscript. The study was initiated by J.E.M.B. and facilitated by A.C.E.

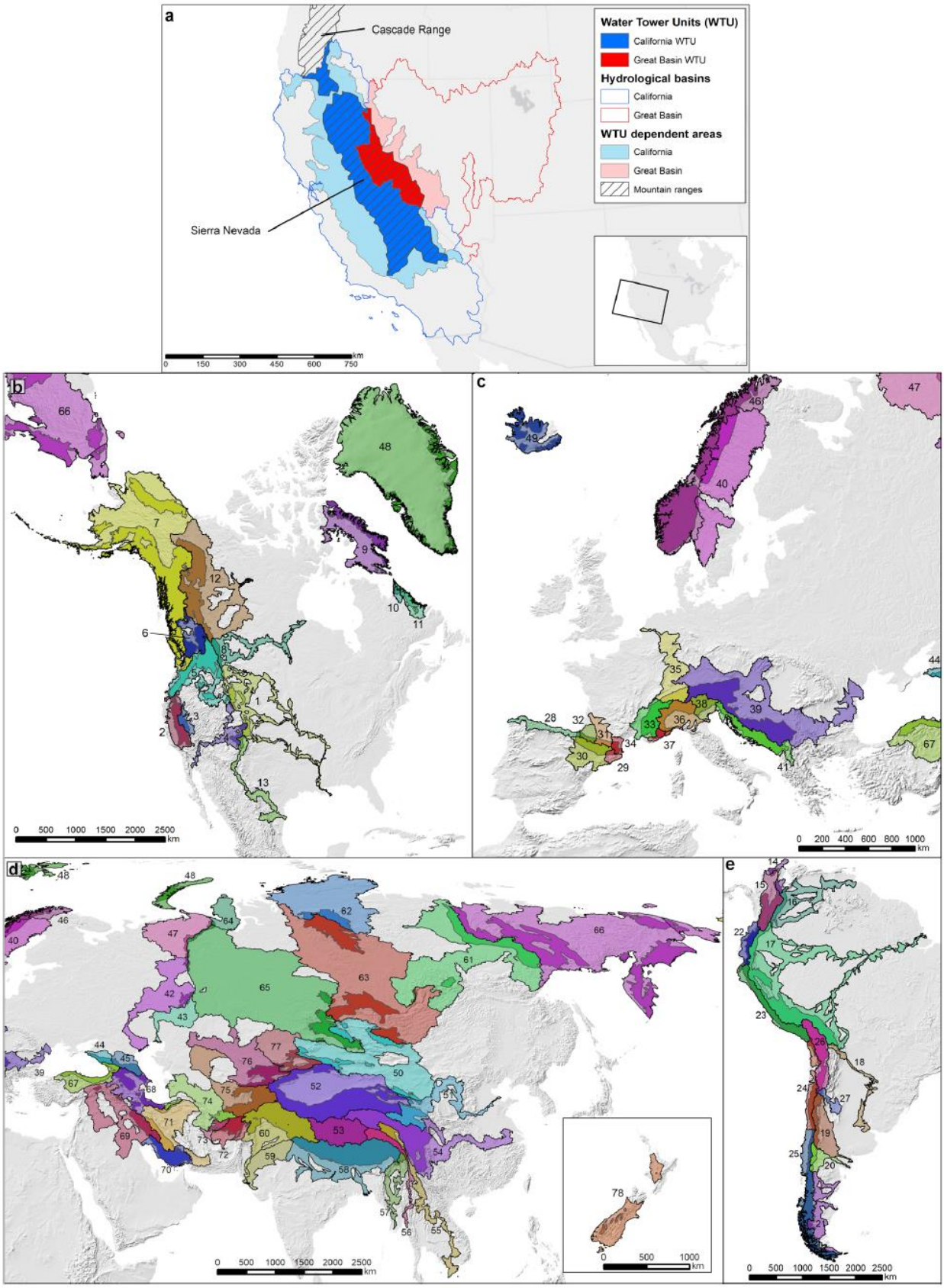

Extended Data Fig. 1 Concept and global spread of WTUs. a, The WTUs are defined as the intersection of Earth's major hydrological basins[5] and mountain ranges[6] meeting predefined

thresholds for ice volume/area and or snow persistence (see Methods section). One WTU can consist of (parts of) multiple mountain ranges and one mountain range can be part of multiple WTUs. The example shows two hydrological basins in North America: the Great Basin (red outline) and California (blue outline). The striped areas indicate two mountain ranges: the Sierra Nevada and the Cascade Range. The intersection of the hydrological basins and the mountain ranges defines the WTUs (dark colours). For example, the Great Basin WTU is defined as the portion of the Sierra Nevada that is part of the Great Basin hydrological basin (dark red), and the California WTU is defined as the portion of the Sierra Nevada that is part of the California hydrological basin as well as a portion of the Cascade Range that is part of the California hydrological basin (dark blue). The WTU's dependent area (light colours) is defined as the sub-basins within the hydrological basin that are overlapping the WTU or downstream of sub-basins overlapping the WTU. **b**–**e**, The WTUs (dark colours) and associated WTU basins (light colours) for all 78 WTUs and WTU basins, grouped by continents: North America (**b**), Europe (**c**), Asia and Oceania (**d**), South America (**e**). Number labels indicate the WTU IDs (see Extended Data Tables 1 and 2 for corresponding names).

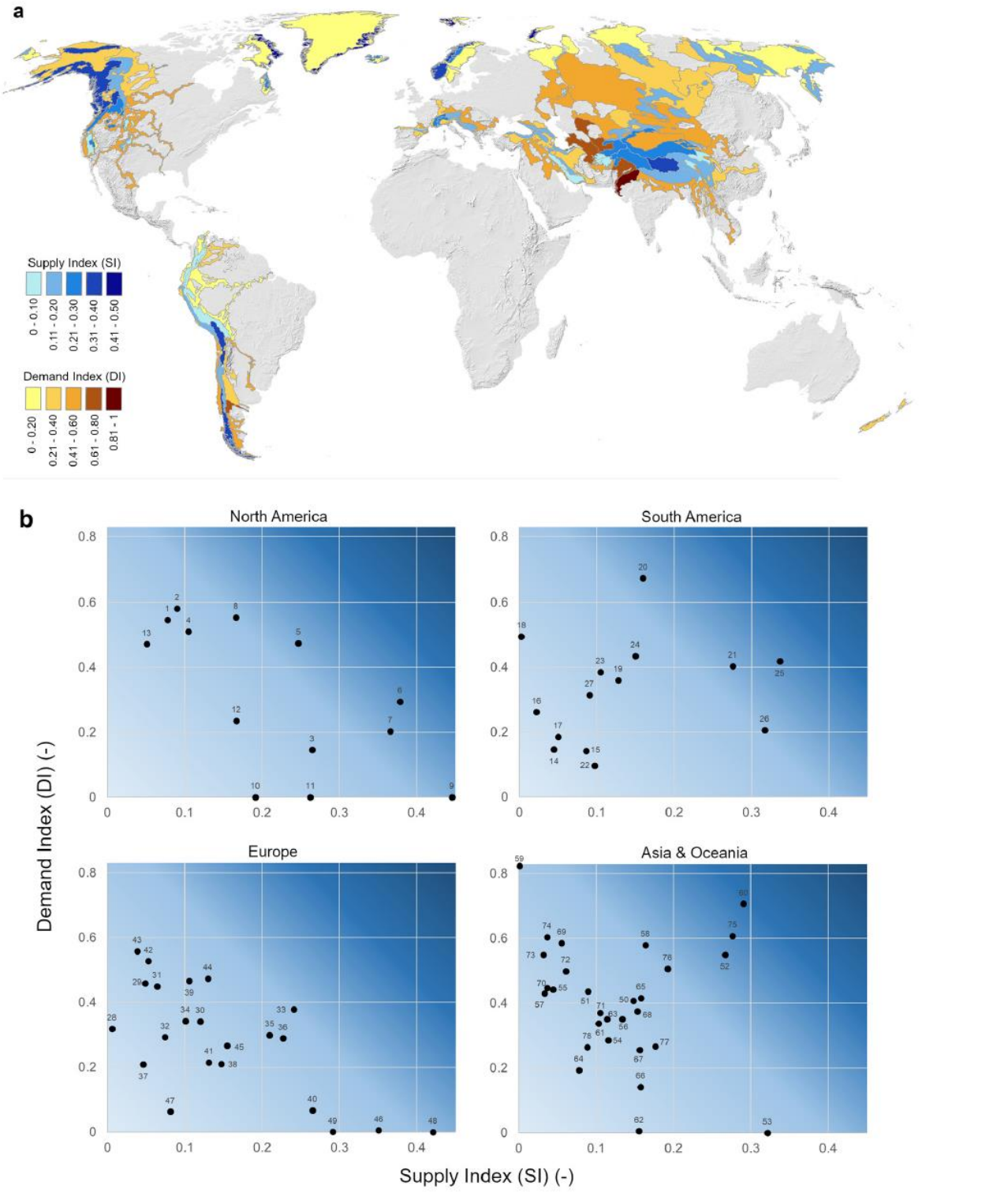

Extended Data Fig. 2 SI and DI. a, The WTU SI (blue colourscale) and downstream DI (brown colourscale) for all 78 WTUs and WTU basins. **b**, Supply index (SI) and demand index (DI) for each WTU grouped per continent. Background colour gradient indicates water tower importance (that is, darker shades represent higher SI and DI values). Points are labelled with WTU IDs (see Extended Data Tables 1 and 2, Extended Data Fig. 1).

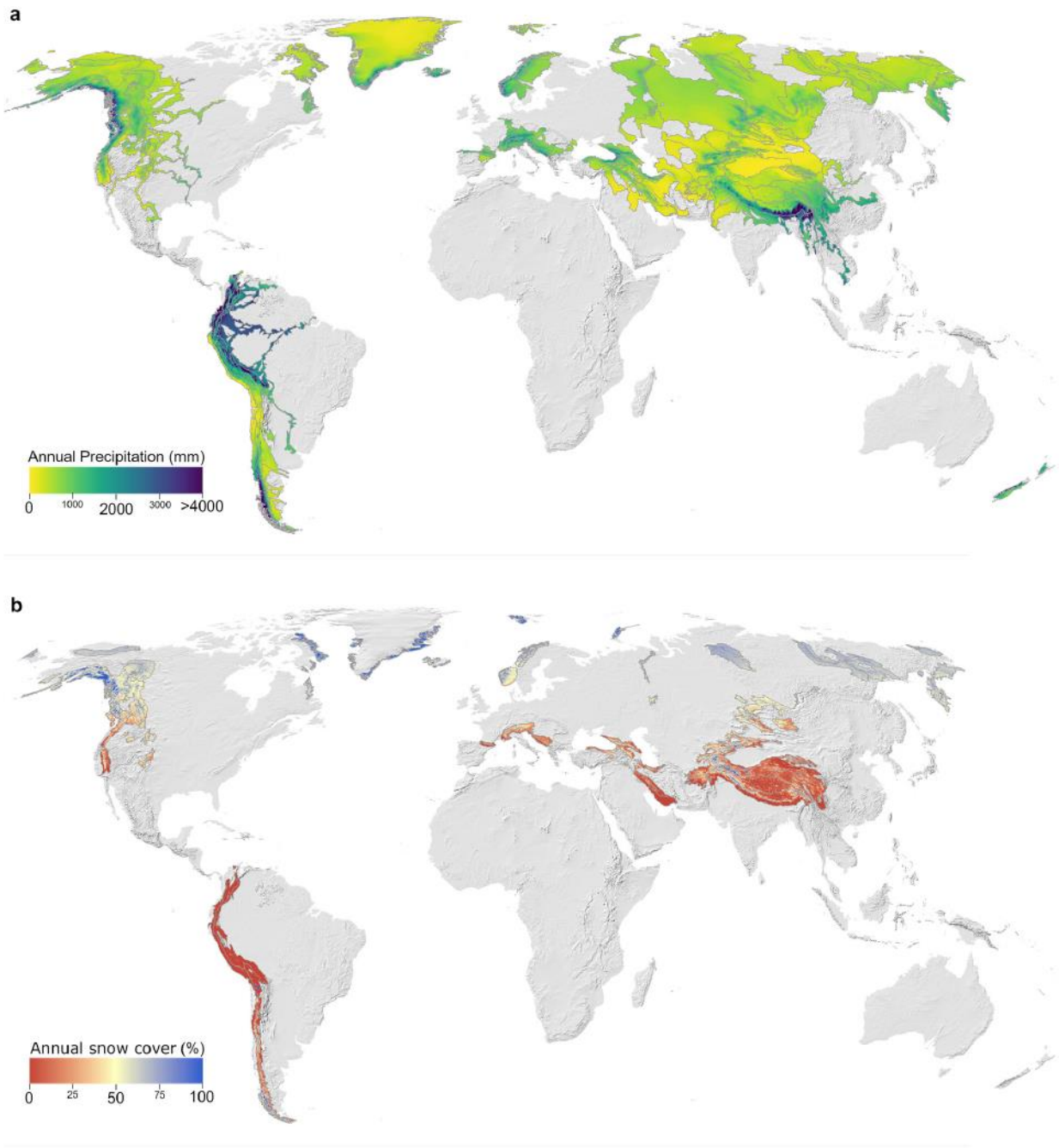

Extended Data Fig. 3 Annual precipitation and snow cover. a, Average annual precipitation between 2001 and 2017, resampled bilinearly to 0.05° resolution based on ERA5[32]. **b**, Average snow persistence between 2001 and 2017, resampled to 0.05° resolution based on MODIS MOD10CM1[7].

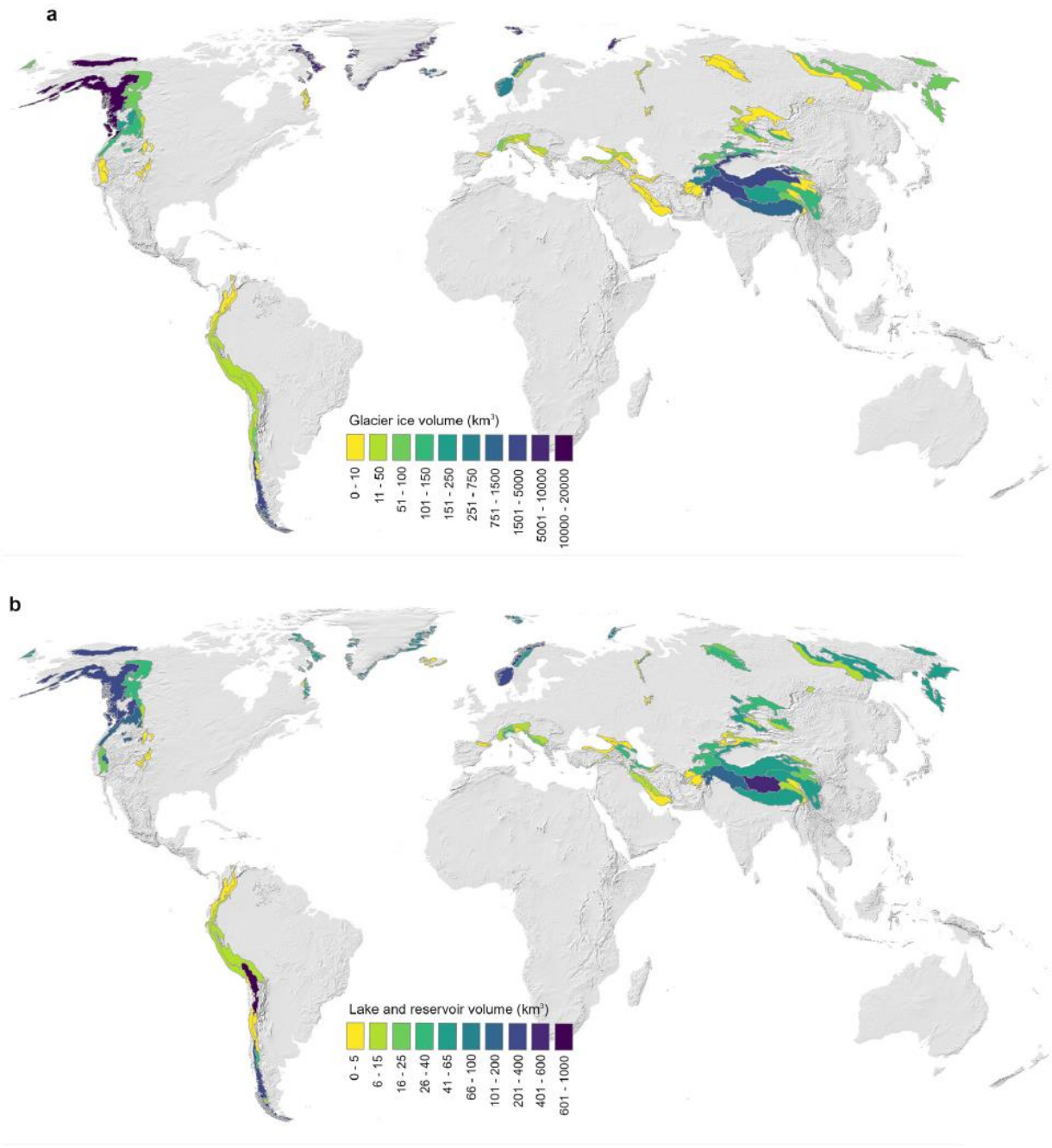

Extended Data Fig. 4 Glacier ice volume and lake and reservoir volume. a, Total aggregated glacier ice volume per WTU[48]. **b**, Total aggregated lake and reservoir water volume per WTU[50].

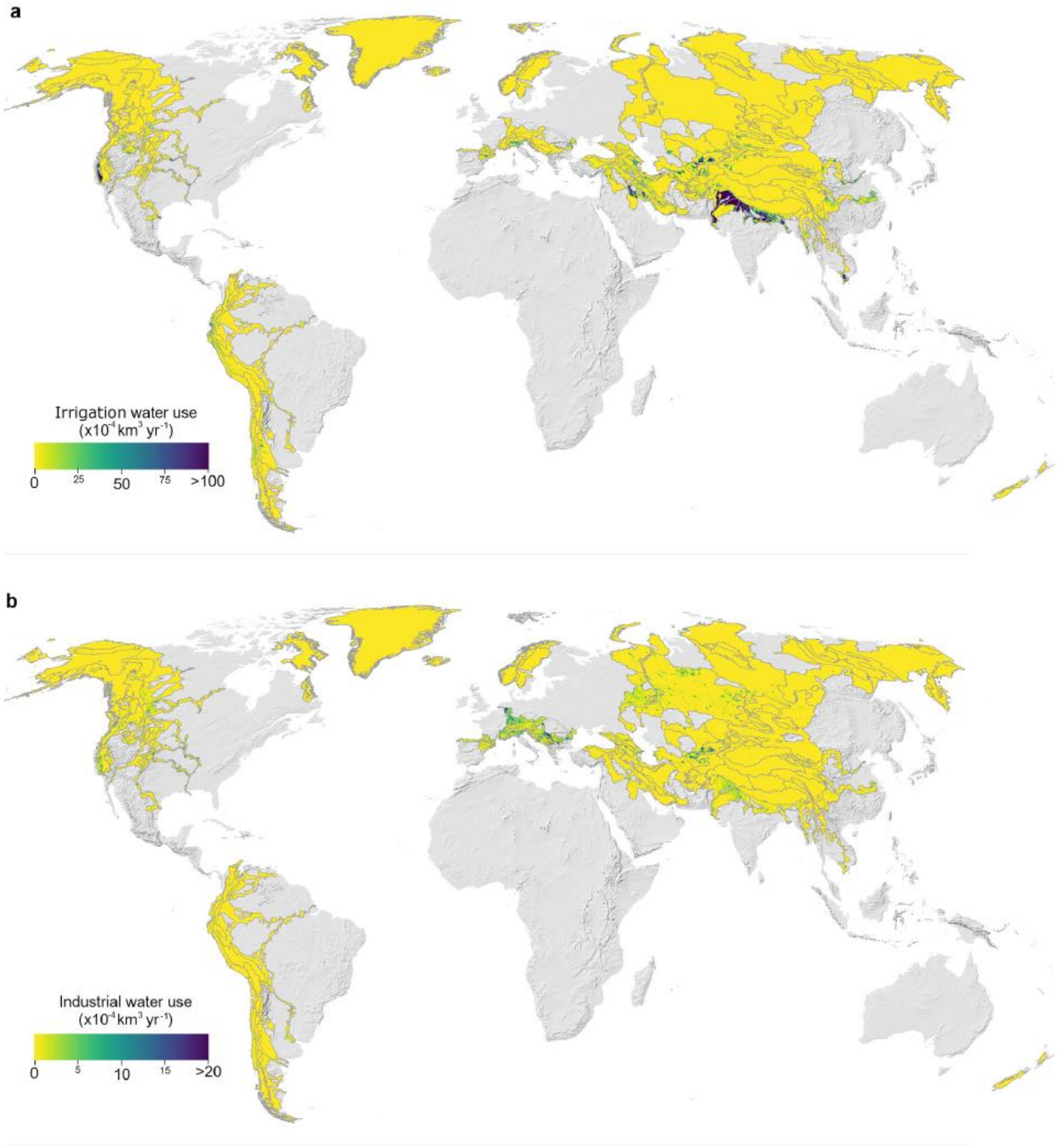

Extended Data Fig. 5 Water use for irrigation and industry. a, Average annual irrigation water use per 0.05 × 0.05° grid cell 2001–2014[33]. **b**, Average annual industrial water use per 0.05 × 0.05° grid cell 2001–2014[33].

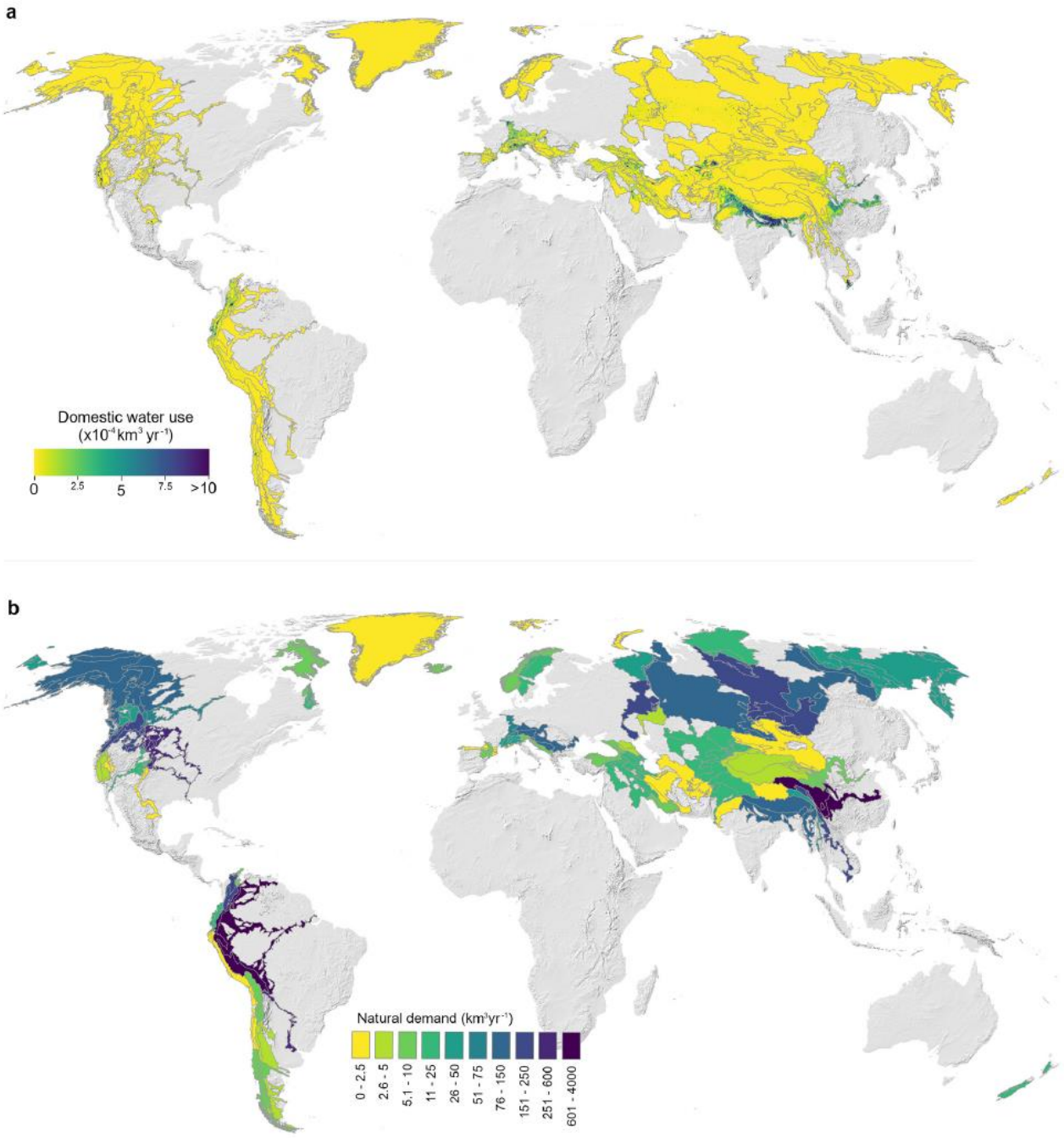

Extended Data Fig. 6 Domestic water use and natural water demand. a, Average annual domestic water use per 0.05 × 0.05° grid cell 2001–2014[33]. **b**, Total aggregated average annual natural water demand 2001–2014 per WTU basin based on the Environmental Flow Requirement[33,51,52].

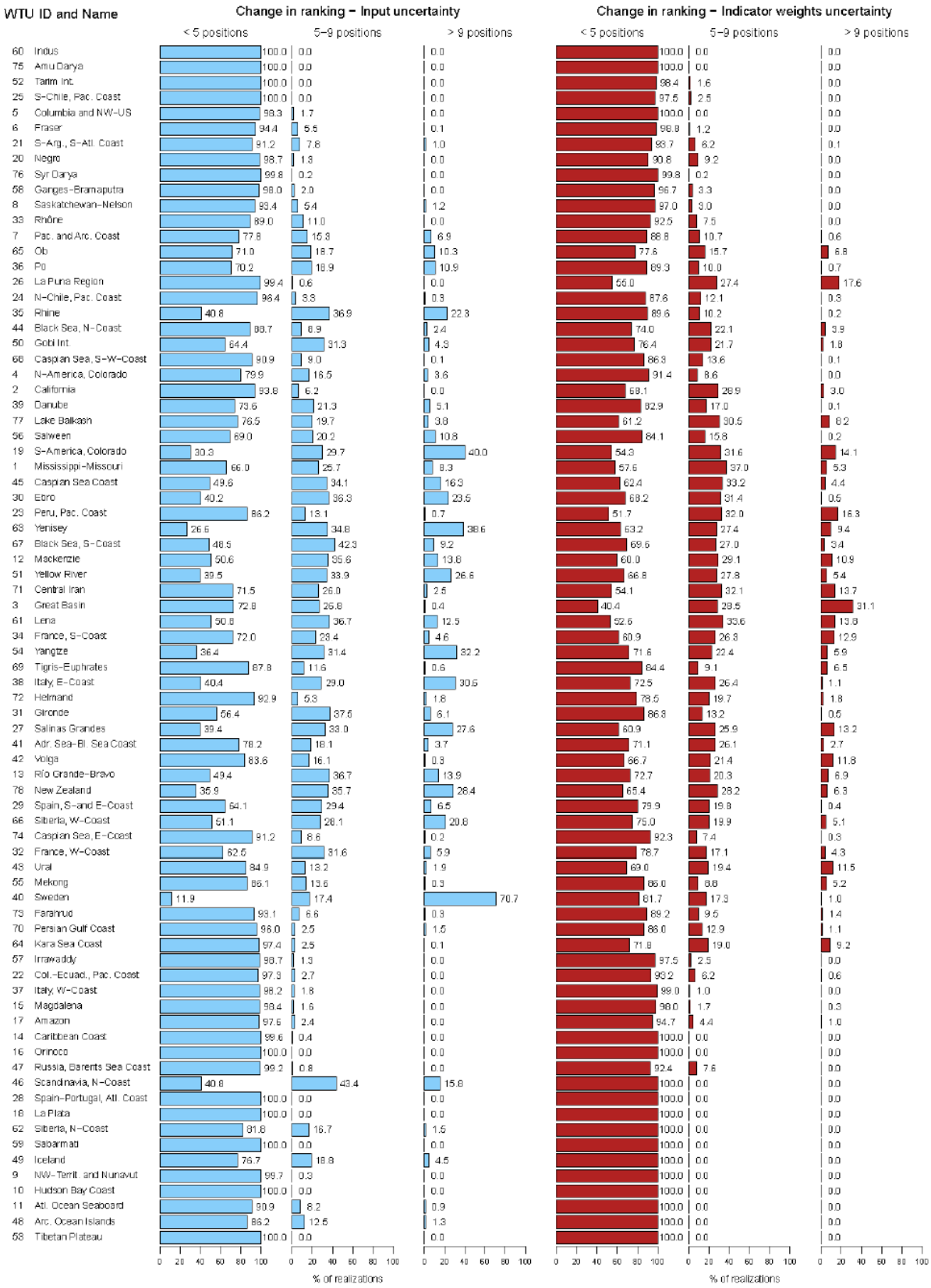

Extended Data Fig. 7 Sensitivity of WTU ranking to uncertainty in input data and indicator weights. Position change in ranking of WTUs by WTI resulting from uncertainty in input data (blue), expressed as a percentage of 1,000 realizations of the WTI index calculation. Position change in

ranking of WTUs by WTI resulting from uncertainty in the weights of individual indicators (red), expressed as a percentage of 10,000 realizations of the WTI index calculation.

Extended Data Table 1 List of WTUs and the GMBA mountain ranges that are (partly) covered by each WTU, for North America and South America

WTU ID	WTU Name	GMBA mountain ranges (partly) covered by WTU
1	Mississippi-Missouri	Bighorn Mountains, Absaroka Range, Crazy Mountains, Lewis Range, Swan Range, Flathead Range, Wind River Range, Front Range, Medicine Bow Mountains, Gore Range, Sawatch Range
2	California	Sierra Nevada, Cascade Range
3	Great Basin	Sierra Nevada
4	N-America, Colorado	San Juan Mountains, Wind River Range, Front Range, Medicine Bow Mountains, Gore Range, Sawatch Range
5	Columbia and NW-US	Absaroka Range, Lewis Range, Swan Range, Mission Range, Flathead Range, Purcell Mountains, Cabinet Mountains, Sawtooth Mountains, Teton Range, Wind River Range, Wallowa Mountains, Cariboo Mountains, Monashee Mountains, Selkirk Mountains, Coast Mountains, Rocky Mountains Calgary, Scrip Range, Cascade Range
6	Fraser	Coast Mountains, Skeena Mountains, Omineca Mountains, Cariboo Mountains, Monashee Mountains, Hazelton Mountains, Rocky Mountains Calgary, Scrip Range, Cascade Range
7	Pac. and Arc. Coast	Chugach Mountains, Kenai Mountains, Alaska Range, Coast Mountains, Aleutian Range, Kodiak and Afognak Island, Alexander Archipelago, Vancouver Island, Brooks Range, Saint Elias Mountains, Wrangell Mountains, Kilbuck Mountains, Talkeetna Mountains, Mackenzie Mountains, Wernecke Mountains, Selwyn Mountains, Pelly Mountains, Skeena Mountains, Stikine Ranges, Cassiar Mountains, Omineca Mountains, Hazelton Mountains, Cascade Range, Olympic Mountains
8	Saskatchewan-Nelson	Lewis Range, Rocky Mountains Calgary
9	NW-Territ. and Nunavut	Baffin Island
10	Hudson Bay Coast	Torngat Mountains
11	Atl. Ocean Seaboard	Torngat Mountains
12	Mackenzie	Mackenzie Mountains, Wernecke Mountains, Selwyn Mountains, Pelly Mountains, Stikine Ranges, Cassiar Mountains, Omineca Mountains, Rocky Mountains Calgary
13	Río Grande-Bravo	San Juan Mountains, Sawatch Range
14	Caribbean Coast	Sierra Nevada de Santa Marta, Cordillera Oriental Colombia Venezuela
15	Magdalena	Sierra Nevada de Santa Marta, Cordillera Central Colombia, Cordillera Oriental Colombia Venezuela
16	Orinoco	Cordillera Oriental Colombia Venezuela
17	Amazon	Cordillera Central Colombia, Cordillera Oriental Colombia Venezuela, Cordillera Central Ecuador, Cordillera Oriental Peru Bolivia, Cordillera Occidental Peru Bolivia Chile, Altiplano
18	La Plata	Cordillera Oriental Peru Bolivia
19	S-America, Colorado	Cordillera principal, Cordillera de Oliva, Cordillera de Ollita, Cerro de Ansilta, Central Volcanic Zone, Cordillera Frontal
20	Negro	Cordillera principal, Northern Patagonian Andes
21	S-Arg., S-Atl. Coast	Cordillera Patagonica Sur, Northern Patagonian Andes, Andes fueginos
22	Col.-Ecuad., Pac. Coast	Cordillera Central Colombia, Cordillera Central Ecuador
23	Peru, Pac. Coast	Cordillera Central Ecuador, Cordillera Occidental Peru Bolivia Chile
24	N-Chile, Pac. Coast	Cordillera principal, Cordillera Occidental Peru Bolivia Chile, Sierra de la Punilla, Sierra de Tatul, Cordillera de Oliva, Cordillera de Ollita, Cerro de Ansilta, Central Volcanic Zone, Cordillera Frontal
25	S-Chile, Pac. Coast	Northern Patagonian Andes, Cordillera Patagonica Sur, Andes fueginos, Cordillera principal, Cordillera Frontal
26	La Puna Region	Cordillera Oriental Peru Bolivia, Cordillera Occidental Peru Bolivia Chile, Altiplano, Central Volcanic Zone, Cordillera Frontal
27	Salinas Grandes	Central Volcanic Zone, Cordillera Frontal

Extended Data Table 2 List of WTUs and the GMBA mountain ranges that are (partly) covered by each WTU, for Europe, Asia and Oceania

WTU ID	WTU Name	GMBA mountain ranges (partly) covered by WTU
28	Spain-Portugal, Atl. Coast	Pyrenees
29	Spain, S-and E-Coast	Pyrenees
30	Ebro	Pyrenees
31	Gironde	Pyrenees
32	France, W-Coast	Pyrenees
33	Rhône	European Alps
34	France, S-Coast	European Alps, Pyrenees
35	Rhine	European Alps
36	Po	European Alps, Pyrenees
37	Italy, W-Coast	European Alps
38	Italy, E-Coast	European Alps
39	Danube	European Alps, Dinaric Alps
40	Sweden	Scandinavian Mountains, Jotunheimen
41	Adr. Sea-Bl. Sea Coast	Dinaric Alps, European Alps
42	Volga	Ural Mountains
43	Ural	Ural Mountains
44	Black Sea, N-Coast	Greater Caucasus
45	Caspian Sea Coast	Greater Caucasus
46	Scandinavia, N-Coast	Scandinavian Mountains, Jotunheimen
47	Russia, Barents Sea Coast	Ural Mountains
48	Arc. Ocean Islands	Svalbard, Greenland Kalaallit Nunaat, Novaya Zemlya
49	Iceland	Iceland
50	Gobi Int.	Haanhöhiy Uul, Borohoro-Shan, Khrebet Dzhungarskiy Alatau, Khrebet Saur, Bogda Shan, Karlik Shan, Tulai Nanshan, Tulai Shan, Zoulang Nanshan, Lenglong Ling, Datong Shan, Türgen Uul, Kuroyskiy Khrebet, Shopshal'skiy Khrebet, Altai Mountains, Tien Shan
51	Yellow River	Lenglong Ling, Datong Shan, Banyan Har Shan, Qionglai Shan, Anyemaqen Shan
52	Tarim Int.	Alayskiy Khrebet, Ferganskiy Khrebet, Terskey Ala Too, Kokshaal Too, Borohoro-Shan, Narat Shan, Horo Shan, Eren Habirga Shan, Danghe Nanshan, Qaidam Shan, Tergun Daba Shan, Yema Shan, Shule Nanshan, Tulai Nanshan, Datong Shan, Pamir, Karakorum, Banyan Har Shan, Anyemaqen Shan, Tibetan Plateau (Xizang Gaoyuan), Kunlun Shan, Tien Shan
53	Tibetan Plateau	Nganglong Kangri, Gangdise Shan, Nyainqentanglha Shan, Tanggula Shan, Tibetan Plateau (Xizang Gaoyuan)
54	Yangtze	Tanggula Shan, Banyan Har Shan, Ningjing Shan, Chola Shan, Shaluli Shan, Daxue Shan, Qionglai Shan, Tibetan Plateau (Xizang Gaoyuan), Yun Range
55	Mekong	Tanggula Shan, Ningjing Shan, Patkai Hills, Mishmi Hills, Tibetan Plateau (Xizang Gaoyuan), Yun Range
56	Salween	Nyainqentanglha Shan, Tanggula Shan, Patkai Hills, Mishmi Hills, Tibetan Plateau (Xizang Gaoyuan)
57	Irrawaddy	Patkai Hills
58	Ganges-Bramaputra	Gangdise Shan, Nyainqentanglha Shan, Tanggula Shan, Himalaya, Patkai Hills, Mishmi Hills
59	Sabarmati	Himalaya
60	Indus	Himalaya, Ladakh Range, Pamir Mountains, Karakorum, Hindu Kush, Nganglong Kangri, Gangdise Shan, Malakand Range, Tibetan Plateau (Xizang Gaoyuan)
61	Lena	Baykal'skiy Khrebet, Khrebet Kodar, Verkhoyanskiy Khrebet, Khrebet Suntar Khayata
62	Siberia, N-Coast	Gory Putorana
63	Yenisey	Haanhöhiy Uul, Shopshal'skiy Khrebet, Kuznetskiy Alatau, Zapadnyy Sayan, Vostochnyy Sayan, Baykal'skiy Khrebet, Gory Putorana
64	Kara Sea Coast	Ural Mountains
65	Ob	Khrebet Saur, Seminskiy Khrebet, Aygulakskiy Khrebet, Kuroyskiy Khrebet, Shopshal'skiy Khrebet, Kuznetskiy Alatau, Zapadnyy Sayan, Altai Mountains, Ural Mountains
66	Siberia, W-Coast	Chukotskiy (Anadyrskiy) Khrebet, Koryakskiy Khrebet, Sredinnyy Khrebet, Verkhoyanskiy Khrebet, Momskiy Khrebet, Khrebet Suntar Khayata, Khrebet Cherskogo, Poluostrov Taygonos
67	Black Sea, S-Coast	Kuzey Anadolu Daglari / Pontus Mountains, Lesser Caucasus, Greater Caucasus
68	Caspian Sea, S-W-Coast	Agri Dagi, Süphan Dagi, Küh-e haye Sabalan, Alborz Mountains, Zagros Mountains, Lesser Caucasus, Greater Caucasus
69	Tigris-Euphrates	Mercan Daglari, Hakkari Daglari, Süphan Dagi, Zagros Mountains
70	Persian Gulf Coast	Zagros Mountains
71	Central Iran	Alborz Mountains, Zagros Mountains
72	Helmand	Hindu Kush
73	Farahrud	Hindu Kush
74	Caspian Sea, E-Coast	Hindu Kush, Alborz Mountains
75	Amu Darya	Zeravshan, Pamir-Alay, Turkestainskiy Khrebet, Gory Baysun Tau, , Pamir, Karakorum, Hindu Kush, Malakand Range
76	Syr Darya	Turkestanskiy Khrebet, Pamir-Alai, Ferganskiy Khrebet, Chatkal'skiy Khrebet, Talas Alatau, Kyrgyz Ala Too, Terskey Ala Too, Kungey Ala Too,
77	Lake Balkash	Kyrgyz Ala Too,, Kungey Ala Too, Ile Alatau, Borohoro-Shan, Dzhungarskiy Alatau, Narat Shan, Tien Shan
78	New Zealand	Ruapehu, Rolleston Range, Two Thumb Range, Liebig Range, Ben Ohau Range, Young Range, Olivine Range, Humboldt Mountains, Richardson Mountains, Livingstone Mountains

Extended Data Table 3 Overview of WTU supply indicators used

Indicator	Symbol	Input	Equation	Reference
Precipitation contribution WTU/basin	P_T	Average annual WTU precipitation sum (2001-2017): P_{WTU} (km^3)	$P_T = P_{WTU} / P_{BAS}$	26
		Average annual basin precipitation sum (2001-2017): P_{BAS} (km^3)		26
Inter-annual variability in precipitation	P_{YV}	Annual WTU precipitation for individual years (2001-2017): P_y (km^3)	$P_{YV} = 1 - ((max(P_y)-min(P_y)) / max(P_y)$	26
Intra-annual variability in precipitation	P_{MV}	Average monthly WTU precipitation sum (2001-2017): P_m (km^3)	$P_{MV} = 1 - ((max(P_m)-min(P_m)) / max(P_m)$	26
Precipitation	P	-	$P = 0.5*(P_{YV}+P_{MV})*P_T$	26
WTU snow cover	S_T	Average annual WTU snow cover: S (-)		5
Inter-annual variability in snow cover	S_{YV}	Annual average WTU snow cover (2001-2017): S_y (-)	$S_{YV} = 1 - ((max(S_y)-min(S_y)) / max(S_y)$	5
Intra-annual variability in snow cover	S_{MV}	Average monthly snow cover (2001-2017): S_m (-)	$S_{MV} = 1 - ((max(S_m)-min(S_m)) / max(S_m)$	5
Snow	S	-	$S = 0.5*(S_{YV}+S_{MV})*S_T$	5
Glacier ice storage	G_S	Total glacier ice volume in WTU: G_V (km^3)	$G_S = G_V / (G_V+P_{WTU})$	42
		Average annual WTU precipitation sum (2001-2017): P_{WTU} (km^3)		26
Glacier melt yield	G_M	Average annual WTU precipitation sum (2001-2017): P_{WTU} (km^3)	$G_M = (P_{GLAC} - B) / (P_{GLAC} - B + P_{WTU})$	26
		Average annual precipitation sum glaciated area (2001-2017): P_{GLAC} (km^3)		26
		WTU average annual glacier mass balance: B (km^3)		14 42
Glaciers	G	-	$G = G_S+G_M$	42
Lake and reservoir storage	L	Total volume stored in lakes and reservoirs in WTUs: S_L (km^3)	$L = S_L / (S_L+P_{WTU})$	44
		Average annual WTU precipitation sum (2001-2017): P_{WTU} (km^3)		26
Final supply index	**SI**		**(P + S + G + L) / 4**	

Extended Data Table 4 Overview of WTU demand indicators used

Indicator	Symbol	Input	Equation	Reference
Domestic demand	D_{DOM}	Average annual downstream domestic water use (2001-2014): $D_{DOM,y}$ (km^3) Average monthly downstream domestic water use (2001-2014): $D_{DOM,m}$ (km^3) Average monthly P-ET (2001-2017) for downstream cells with domestic demand above threshold: $WA_{DOM,m}$ (km^3) Threshold is $1*10^{-6}$ km^3 per 0.05° grid cell	$\Sigma (D_{DOM,m} - WA_{DOM,m}) / D_{DOM,y}$	58
Industrial demand	D_{IND}	Average annual downstream industrial water use (2001-2014): $D_{IND,y}$ (km^3) Average monthly downstream industrial water use (2001-2014): $D_{IND,m}$ (km^3) Average monthly P-ET (2001-2017) for downstream cells with industrial demand above threshold: $WA_{IND,m}$ (km^3) Threshold is $1*10^{-6}$ km^3 per 0.05° grid cell	$\Sigma (D_{IND,m} - WA_{IND,m}) / D_{IND,y}$	58
Irrigation demand	D_{IRR}	Average annual downstream irrigation water use (2001-2014): $D_{IRR,y}$ (km^3) Average monthly downstream irrigation water use (2001-2014): $D_{IRR,m}$ (km^3) Average monthly P-ET (2001-2017) for downstream cells with irrigation demand above threshold: $WA_{IRR,m}$ (km^3) Threshold is $1*10^{-6}$ km^3 per 0.05° grid cell	$\Sigma (D_{IRR,m} - WA_{IRR,m}) / D_{IRR,y}$	58
Natural demand	D_{NAT}	Average annual Environmental Flow Requirement at river basin outlet (2001-2014): $D_{NAT,y}$ (km^3) Average monthly Enviromental Flow Requirement at river basin outlet (2001-2014): $D_{NAT,m}$ (km^3) Average monthly P-ET for downstream basin (2001-2017): $WA_{NAT,m}$ (km^3)	$\Sigma (D_{NAT,m} - WA_{NAT,m}) / D_{NAT,y}$	46,58,64
Final demand index	**DI**		**$(D_{IRR} + D_{IND} + D_{DOM} + D_{NAT}) / 4$**	